

Supplementary Information

Performance-oriented multistage design for multi-principal element alloys with low cost yet high efficiency

Jia Li, Baobin Xie, Li Li, Bin Liu, Yong Liu, Dmitry Shaysultanov, Qihong Fang, Nikita Stepanov, and Peter K. Liaw

Supplementary Text 1

Yield strength of MPEAs

The lattice-friction stress introduced by a single element in MPEAs can be expressed as

$$\sigma_f^i = AGc_i^{2/3} \delta_i^{4/3} \quad (1)$$

where A is a non-dimensional constant, which is equal to 0.04. G is the shear modulus of the material, which is obtained from the experiments. c_i is the atomic fraction of individual principal elements in MPEAs. δ_i represents the mismatch parameter introduced by an element i , which is correlated with the elastic mismatch and the atomic-size mismatch, $\delta_i = \xi(\delta G_i^2 + \beta^2 \delta r_i^2)^{1/2}$, where ξ is equal to 2.5 for BCC MPEAs, and 1 for FCC MPEAs. β is dependent on the type of the dislocation, which is equal to 4 for BCC MPEAs, and 16 for FCC MPEAs, respectively. The elastic mismatch, δG_i , and the atomic-size mismatch, δr_i , introduced by the element, i , can be written as $\delta r_i = (\delta r_{ijklm}^{ave} - \delta r_{jklm}^{ave}) / \delta c_i$, and $\delta G_i = (\delta G_{ijklm}^{ave} - \delta G_{jklm}^{ave}) / \delta c_i$, where δr_{ijklm}^{ave} and δG_{ijklm}^{ave} denote the average atomic-size mismatch and elastic mismatch of the $ijklm$ MPEA. δr_{jklm}^{ave} and δG_{jklm}^{ave} represent the average atomic-size mismatch and elastic mismatch of the $jklm$ MPEA. δc_i represents the atomic-fraction difference of the element, i , between the $ijklm$ and $jklm$ MPEAs.

The various elements are assumed to be distributed uniformly in MPEAs. The average elastic mismatch and atomic-size mismatch of MPEAs can be expressed as

$$\delta r^{ave} = \sum_i^n \sum_j^n c_i c_j \delta r_{ij} = (c_1, c_2, L, c_n) \begin{pmatrix} \delta r_{11} & \delta r_{12} & L & \delta r_{1n} \\ \delta r_{21} & \delta r_{22} & L & \delta r_{2n} \\ M & L & O & M \\ \delta r_{n1} & \delta r_{n2} & L & \delta r_{nn} \end{pmatrix} \begin{pmatrix} c_1 \\ c_2 \\ M \\ c_n \end{pmatrix} \quad (2)$$

$$\delta G^{ave} = \sum_i^n \sum_j^n c_i c_j \delta G_{ij} = (c_1, c_2, L, c_n) \begin{pmatrix} \delta G_{11} & \delta G_{12} & L & \delta G_{1n} \\ \delta G_{21} & \delta G_{22} & L & \delta G_{2n} \\ M & L & O & M \\ \delta G_{n1} & \delta G_{n2} & L & \delta G_{nn} \end{pmatrix} \begin{pmatrix} c_1 \\ c_2 \\ M \\ c_n \end{pmatrix} \quad (3)$$

where δG_{ij} and δr_{ij} are the elastic mismatch and the atomic-size mismatch between the atoms, i and j , which can be expressed as $\delta r_{ij} = 2(r_i - r_j) / (r_i + r_j)$, and $\delta G_{ij} = 2(G_i - G_j) / (G_i + G_j)$, where r_i and r_j are the atomic radii, G_i and G_j are the shear moduli of pure metals i and j , respectively.

Finally, the lattice-friction stress in MPEAs can be expressed through the Vegard's law based on the lattice-friction stress introduced by each element, $\sigma_f = \sum c_i \sigma_f^i$. The grain-boundary strengthening depends on the size of the grain obtained by experimental observations, which can be described by the classical Hall-Petch strengthening relationship as follows, $\sigma_{gb} = k / \sqrt{d}$, where k represents the strengthening coefficient of the material, and d is the average grain size. Therefore, the yield stresses of MPEAs can be expressed as the sum of the lattice-friction stress and the grain-boundary strengthening:

$$\sigma_y = \sigma_f + \sigma_{gb} \quad (4)$$

For dual-phase MPEAs, we employed the rule of the mixture to calculate the overall yield strength

$$\sigma_{\text{mix}} = f_\alpha \sigma_\alpha + f_\beta \sigma_\beta \quad (5)$$

where σ_{mix} is the overall yield strength of the two-phase mixed system, σ_α represents the yield strength of the α phase, and σ_β denotes the yield strength of the β phase. f_α and f_β represent the volume fractions of α and β phases, respectively.

Machine learning algorithm

Five folds cross-validation strategy: The appearance of over fitting and under fitting issue makes us have a wrong understanding of the performance of machine learning algorithm. Here, to accurately evaluate KNN, SVM and DT algorithms and improve the performance of these machine learning algorithms, five folds cross-validation strategy is adopted as shown in Fig. S2. In fact, the times of cross-validation has significant influence on evaluating the performance of machine learning algorithms. The less times of cross-validation probably will produce the large variation of standard deviation due to random division of data set. However, the excessive times will cause low efficiency. From the previous literature, we choose five folds cross validation strategy.^{1, 2} Firstly, the whole data set is divided into five equal nearly sub-data sets assigned by IDs (SD1, SD2, SD3, SD4, and SD5). Each sub-data set is adopted once as the testing data set and the left four data sets are used as training data sets. Using this strategy, the machine learning algorithm can be trained and tested five times in entire data set. The final accuracy value of each machine learning algorithm is the average of five testing results. The validation process gives us a reliable and accurate evaluation on machine learning algorithms. Such k folds cross-validation

method are also used in the previous work.¹ This average accuracy is correct enough to evaluate the performance of each machine learning algorithm.

Early-stopping strategy: When we try to train ANN model, we usually hope to obtain the best generalization performance. However, all standard ANN structures are easy to encounter over-fitting problem: when the network performs better and better in the training set, in fact, at a certain moment, its performance on the test set has begun to deteriorate. Early-stopping strategy³ is a widely used method. Its basic guideline is to calculate the performance of the model on the validation set during training stage. When the accuracy of the model on the validation set begins to decline, and then we stop training process, which can avoid the over-fitting problem caused by continuous training.

KNN: The KNN algorithm is perhaps the most popular and straightforward classifier in machine learning. The samples are classified by querying from nearest neighbors, which are in the training dataset. Under the premise of the sufficient random access memory, this algorithm is usually useful to solve not only low-dimensional binary classification problems, but also high-dimensional multi-labels classification problems. To explain the simple idea of the KNN algorithm, In Fig. S3, the 4-nearest neighbors algorithm is described in a two-dimensional space. For the unknown sample 2, it can be seen that all four of its nearest neighbors are class Δ , so the classification decision related to the unknown sample 2 is the class, Δ . However, the circumstance for the unknown sample 1 is a bit complex since the nearest neighbors of the sample 1 are three of class, \times , and one of class, Δ . The final classification decision for the unknown sample 1 should be made comprehensively from the distance and features weight. In Fig. S3, the pseudo code shows the general flow of the KNN algorithm.

From Fig. S3, it can be found that not only the K value, but also distance metrics have great influence on the classification accuracy. Assuming that the training samples have n features (X_{train}), the general distance metrics between the training sample point and the sample point to be classified (X_{test}) can be written as:

$$d(X_{train}, X_{test}) = \sum_{i=1}^n \omega_i d(X_{train}^i - X_{test}^i) \quad (6)$$

where ω_i represents the weight of each feature. Several common distance metrics, including the Euclidean distance, cosine distance, and correlation distance, are evaluated in the present work.

DT: The DT algorithm is a common supervised learning method mainly used for solving classification problems. It can simulate the process of human decision-making, which usually depends on the observation of the input features and the existing experience. Meanwhile, as a kind of the greedy algorithm, every input feature is deeply mined for the most accurate classification result.⁴ A simple example of the DT algorithm is presented as shown in Fig. S4. The architecture of DT consists of root nodes, branches, internal nodes and leaf nodes, which are arranged from top to bottom like a tree structure. The root node is at the top, and the internal nodes of the second layer are connected with the root node through branches. Internal nodes can continuously generate new internal nodes through branches. When new internal nodes cannot be generated, and each leaf node (terminal nodes) are generated on the branches. It indicates that the final decisions have been made.⁵ The pseudo code in Fig. S4 shows the general flow of the decision algorithm.

The accuracy of a decision-tree algorithm can be greatly improved by choosing an appropriate splitting criterion at nodes, which usually depends on the “trial and error” method. Some common splitting criteria, including the Gini’s diversity index, the Twoing rule and Maximum deviance reduction,⁶ which are also evaluated in the present work.

SVM: The SVM algorithm is an effective machine learning method to solve classification problems with high dimensional features. A general flow shown in Fig. S5 is to solve a classification problem using the SVM algorithm. The basic idea of SVM is to search for the linear classifier (hyper-space) with the maximum distance in the high dimensional feature space, which makes it different from the conventional perceptron (the hyperspace, which can correctly label a training data set; not required to ensure the maximum distance).⁷ Given a training data set of $T = \{(x_1, y_1), (x_2, y_2), (x_3, y_3), \dots, (x_n, y_n)\}$, where $x_i \in R^n$ represents n features of each sample, and $y_i \in \{-1, 1\}$ denotes two classes of the sample. Define the distance between the support vector and hyper-plane:

$$\theta = \min_{i=1,2,\dots,n} y_i \left(\frac{\omega}{\|\omega\|} \cdot x_i + \frac{b}{\|\omega\|} \right) \quad (7)$$

Based on the basic idea about the SVM algorithm, the task for the optimal hyper-space can be transformed into an optimization problem under certain constraints. Here, a Lagrange multiplier is introduced to construct a Lagrange function for solving the optimization problem, which can be written:

$$L(\omega, b, \alpha) = \frac{1}{2} \|\omega\|^2 - \sum_{i=1}^n \alpha_i (y_i (\omega \cdot x_i + b) - 1) \quad (8)$$

Then, by utilizing the duality of the Lagrange function, setting the partial derivative of the Lagrange function to ω and b to 0, introducing penalty parameter, C, and embedding the kernel function, $K(x, y)$, the SVM algorithm can be formulated as follows:

$$\begin{cases} \min_{\alpha} \frac{1}{2} \sum_{i=1}^n \sum_{j=1}^n \alpha_i \alpha_j y_i y_j K(\mathbf{x}_i, \mathbf{x}_j) - \sum_{i=1}^n \alpha_i \\ \sum_{i=1}^n \alpha_i y_i = 0 \\ \mathbf{b}^* = y_j - \sum_{i=1}^n \alpha_i^* y_i K(\mathbf{x}_i, \mathbf{x}_j) \\ 0 \leq \alpha_i \leq C, i = 1, 2, 3, \dots, n \end{cases} \quad (9)$$

where α^* represents the optimal Lagrange multiplier. Several common kernel functions, such as linear kernel, quadratic kernel, cubic kernel and Gaussian kernel for the SVM algorithm.

ANN: The architecture of ANN is a fully-connected network composed of an input layer, several hidden layers, and an output layer. The main function of the input layer is to perceive the external world by receiving some information, such as some specific data or signals. These information can be accepted in the form of real numbers, binary values, and integers. The following step is in the hidden layers. When the information passes through the hidden layers, the features are extracted and processed by neurons. The hidden layers undertake the most of calculations in whole internal processing. The output layer makes the final decision about the input information via integrating the results of the previous layers.⁸

Each layer is composed of neurons, which are fully connected with the input vector. Here, it should be noted that there is no connection between neurons in each layer and no cross-layer connection between neurons in different layers. All neurons in the ANN framework are forced to connect forward. In other words, the information transmission is continuous, and the recurrent or backward connection between neurons does not exist. The output of the j th neuron in the hidden layer, a_j , can be given via the following linear equation:

$$a_j = \sum_{i=1}^n \omega_i \cdot x_i + b_j \quad (10)$$

where ω_i represents the weights relevant to the input variable, x_i , and b_j denotes the bias term, which is used to help activate the neurons in the case of that $\sum_{i=1}^n x_i \cdot \omega_i$ equals zero. Furthermore, in a classification problem, the Softmax activation function is generally used in the output layer, which is defined as:

$$\text{Softmax}(z_i) = \frac{e^{z_i}}{\sum_{j=1}^n e^{z_j}} \quad (11)$$

where z_i represents the output of i th node in the output layer, and n is the number of classes.

Lastly, the cross-entropy function is used as the loss function, which is given by the formula:

$$\text{cross_entropy} = -\sum_{i=1}^n q_i \log(p_i) \quad (12)$$

where q_i denotes the target class, and p_i represents the prediction probability. In addition, error (target output - predicted output) back propagation strategy is employed to update the ω_i and b_j continuously.⁹ A typical ANN architecture for phase prediction, which consists of an input layer, two hidden layers, and one output layer, is illustrated in Fig. S6.

Supplementary Text 2

Prediction of the optimal composition in the Al-Fe-Co-Cr-Ni-Mn system

Here, the optimal composition in the Al-Fe-Co-Cr-Ni-Mn system with high strength and good elongation is predicted by our proposed multistage design method. Based on the experimental data reported so far, we determine the target strength (> 800 MPa) and elongation ($> 10\%$). In view of the fact that the alloy phase structure transformation from the single FCC structure to a duplex FCC plus BCC structure and then a single BCC structure with increasing the Al concentration in the Al-Fe-Co-Cr-Ni-Mn system. Thus, to meet the target strength, we obtain the initial composition scope of Al using a mathematical model by assuming the alloy is a single FCC phase structure. Considering elongation criteria ($> 10\%$), we further narrow the component range of Al by our elongation prediction model. Subsequently, we determine the phase structure and the corresponding volume fraction in the selected component range by phase prediction model. Here, the detailed phase structure prediction is provided in Main Text “Phase prediction”. For phase volume fraction prediction, we establish the “composition - FCC/BCC volume fraction” data set using data augmentation strategy based on the reported research.¹⁰ The data set can be found in Data S5. Then, a machine learning model is developed via the ANN algorithm for predicting phase fraction in the Al-Fe-Co-Cr-Ni-Mn system. The performance of the model is illustrated in Fig. S7. Then, we compute the yield strength and elongation of candidate MPEAs by the FP avenue, as presented in the Table S6. Finally, a new multi-phase MPEA ($\text{Al}_{0.63}\text{Co}_{0.95}\text{Cr}_{0.95}\text{FeMn}_{0.74}\text{Ni}$) with the optimal combination of strength and elongation are determined. The errors between the predicted and experimental results demonstrated in Table S7 are within 10.0%, indicating that the proposed approach can accurately predict the properties of MPEAs.

Supplementary Text 3

Performance for KNN, DT, SVM, and ANN on phase prediction

We exhibit the evaluation of the prediction accuracy using KNN with various distance metrics / K values in Fig. S8a. It proves that both the K value and distance metric have great influence on the final prediction accuracy. For the phase selection of MPEAs, we do not impose the previous knowledge on KNN as a limitation so as to only consider the effect of KNN itself on the classification result, that is, the weight of each input physical feature is ignored. The final classification result of KNN completely depends on the proportion of different phases in K nearest neighbors. For most of the distance metrics, when the K value is smaller, the KNN achieves higher prediction accuracy. Furthermore, the optimal K value/distance metric are selected for the phase prediction of MPEAs with various input features. The classification result in the form of the confusion matrix is shown in Figs. S8b-d. Here, the squares marked by green color represent the correct classification, and the number in them denotes the percentage of the correct classified samples in the total number of samples. From the confusion matrix, the reduction of input features can effectively improve the prediction accuracy on BCC and FCC structures whereas decreasing the accuracy on the BCC + FCC structure, which also indicates that the formation rule of a multi-phase structure is complex.

We evaluate the prediction accuracy of the DT algorithm with various input features on the condition of different split criteria in the form of a Receiver Operating Characteristic (ROC) curve ¹¹ (The maximum deviance reduction, Gini's diversity index, and Twoing rule are the best split criteria for twelve/eleven/nine input features) in Figs. S9a-c. The ROC curve shows the competition between the true positive rate (TPR) and false positive rate (FPR) for different thresholds of classifiers. Meanwhile, the ROC curve can easily find out the ability of a classifier

to recognize samples at a certain threshold. The optimal threshold, which has the highest classification accuracy, can be obtained. Furthermore, the performance of the classifier in the regions of high sensitivity and high specificity can be evaluated. The area marked by blue shows an estimation of the overall performance of the classifier. A larger area indicates more accuracy for classification results. The point marked by red color shows the performance of the current classifier. It can be seen that the DT algorithm has the lower prediction accuracy than that of the KNN algorithm. This is because the DT algorithm, as a greedy algorithm, will over-exploit a single physical feature and easily ignores the correlation between input features, which makes the BCC + FCC structure more difficult to be predicted.

The classification results for the phase selection of MPEAs with twelve, eleven, and nine features via the Cubic kernel SVM algorithm (the best kernel for twelve/eleven/nine input features) are shown in Figs. S10a-c. Among them, the highest prediction accuracy is 81.2%, using the Cubic kernel SVM algorithm with nine features. Though the result reflects that the proposed feature engineering is feasible and effective for the Cubic kernel function in searching for the optimal hyperplane, such prediction accuracy still cannot perfectly solve the problem of phase selections in MPEAs. In fact, the SVM algorithm cannot effectively solve the problem of multi-label classification in essence. The ultimate goal of the SVM algorithm is to search for the optimal hyper-plane, which can completely distinguish different classes. Such a mechanism gives a great advantage, using SVM in binary classification problems. However, when applying the SVM algorithm to solve multi-label classification results, it has to transform them into multiple binary classification problems. Of course, when there are serious overlaps between the classes, the SVM algorithm cannot completely distinguish different classes. Therefore, errors accumulate in each search for the optimal hyper-plane until all classes are distinguished, which

leads to the low prediction accuracy of applying the SVM algorithm to solve the problem of the phase selection of MPEAs.

We present the confusion matrix plotted on the basis of the result of the ANN algorithm for the classification accuracy with twelve, eleven, and nine input features, respectively, in Figs. S11a-c. Generally, the ANN algorithm is sensitive with input features, and the redundant feature would significantly obstruct the efficiency and accuracy of the ANN model. Therefore, feature engineering becomes an indispensable step before using the ANN algorithm. Here, it can be seen that a regular feature engineering mean (11 features) cannot improve the prediction accuracy (the average accuracy of training data set, validation data set and testing data set, i.e., the average accuracy of the entire data set) whereas the accuracy of the ANN model reaches 89.1% based on the physics-based feature engineering strategy. These results not only demonstrate that the ANN model can accurately predict the phase selection of MPEAs, but also more importantly, indicate the feasibility and importance of the present physics-based feature engineering strategy.

Supplementary Text 4

Elongation prediction

We have calculated the yield strength of the MPEAs through the proposed multistage-design approach integrating machine learning, physical law and mathematical model. The mathematical model can take into account the microstructural features and crystal structure features of MPEAs, which is a very important bridge to relate fundamental material properties to macroscopic material behavior. However, a quantitative correlation between atomic scale deformation and macroscale elongation remains extremely challenging, due to the complex deformation and fracture mechanisms in MPEAs, including (i) the movement of the defect, such as the dislocation, void, and grain boundary, whose distribution and density are usually uncertain; (ii) the interaction between defects and between defect and microstructure, such as dislocation-void, and dislocation-distorted crystal structure; (iii) distribution and concentration of elements would affect the defect structure and motion; (iv) studies on the nucleation and propagation of voids and microcracks are still rare. In view of the fact that there is currently no suitable mathematical model to predict the elongation of MPEAs, we have to predict their elongation by embedding physical laws into machine learning. To predict elongation of MPEAs by adopting machine learning, the data set consisting of 64 entries (Data S6) is established by gathering the previous experimental results. In addition, in order to avoid the performance difference caused by the variation of process parameters and test conditions, the MPEAs in the data set are all produced by arc-melting and the elongation of the MPEA is measured under tension condition. We present the performance curve during the training stage using ANN in Fig. S12a. The mean squared error (MSE)¹² between the predicted and experimental values is as a loss function. Meanwhile, the early-stopping strategy is used to prevent the over-fitting problem. We further plots the

prediction results of a training data set, validation data set, test data set, and all data, respectively, as shown in Fig. S12b. The dotted line represents that the predicted value is completely consistent with the experiments. Furthermore, we linearly fit the predicted value with the experimental result in the form of the solid line. By comparing the distance between the solid lines and dotted lines, it can be found that our ANN model performs well on predicting the elongation of the MPEA.

Supplementary Text 5

Additional validation of the proposed multistage-design approach

In order to further demonstrate the validity comprehensively of the proposed multistage-design approach, the additional tensile experiment of $\text{Al}_{0.55}\text{Co}_{0.9}\text{CrFe}0.95\text{Mn}_{0.8}\text{Ni}_{0.8}$ MPEA has been carried out. The results show a yield strength of 691 MPa, the ultimate tensile strength of 1,029 MPa, and the elongation of 13.4% for $\text{Al}_{0.55}\text{Co}_{0.9}\text{CrFe}0.95\text{Mn}_{0.8}\text{Ni}_{0.8}$ MPEA (Fig. S13). These results are consistent with our predictions. The deviations between the predicted and experimental results exhibited in Table S8 are also within 10.0%, further demonstrating the proposed multistage-design approach can accurately predict the properties of MPEAs.

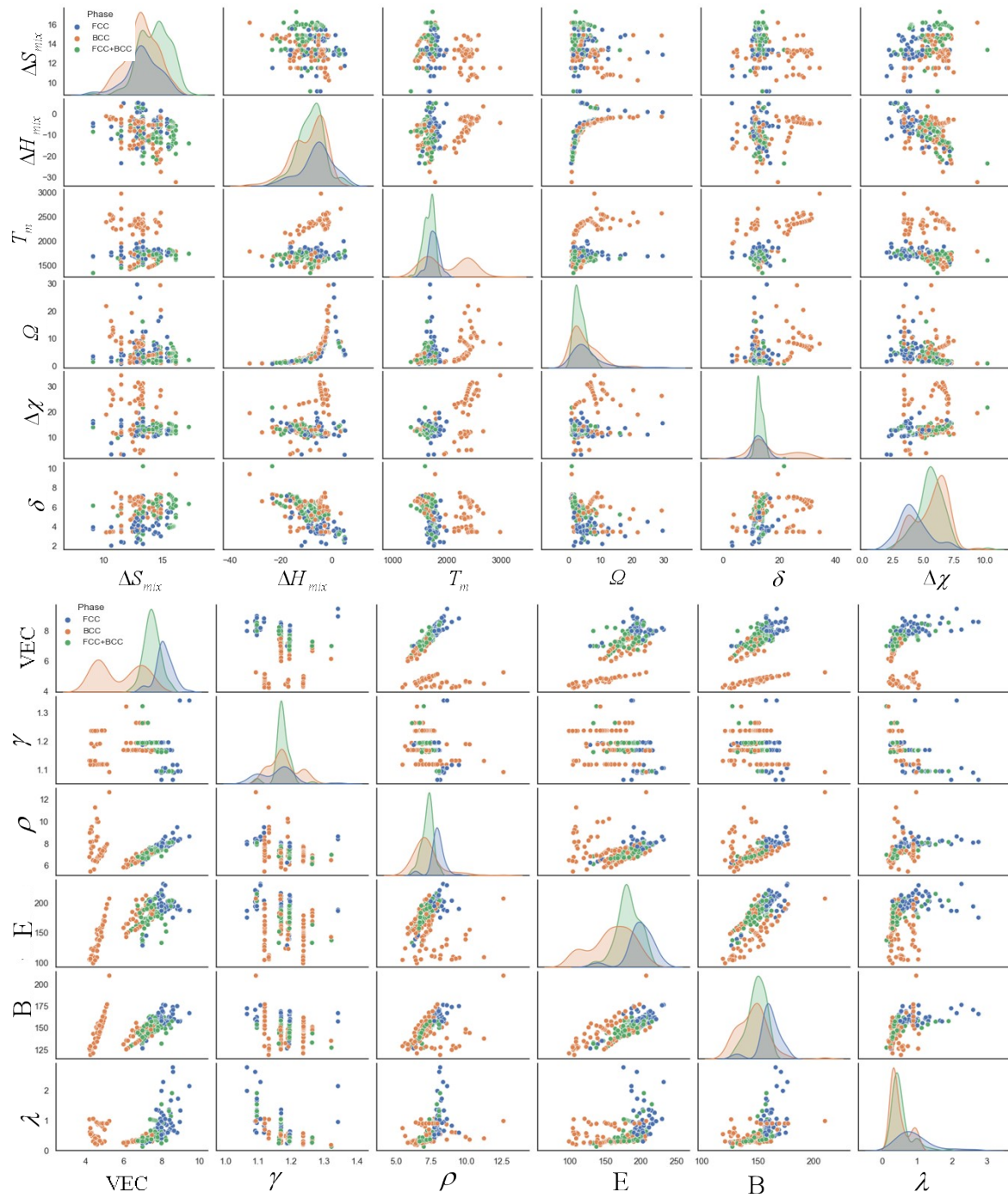


Fig. S1. The correlation between 12 features that are related to the phase selection of MPEAs in the form of scatter matrix. The circles in scatter matrix are marked by different colors representing various phases.

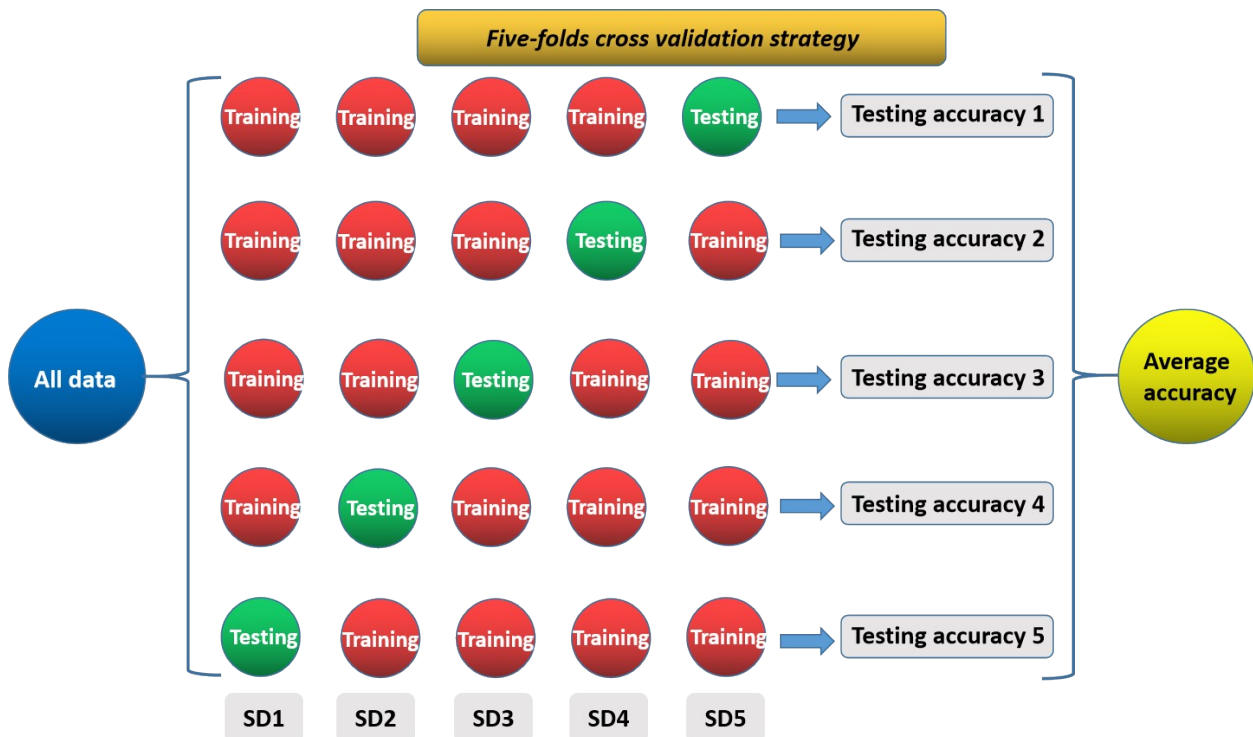


Fig. S2. Five folds cross-validation strategy for SVM, KNN, and DT algorithm.

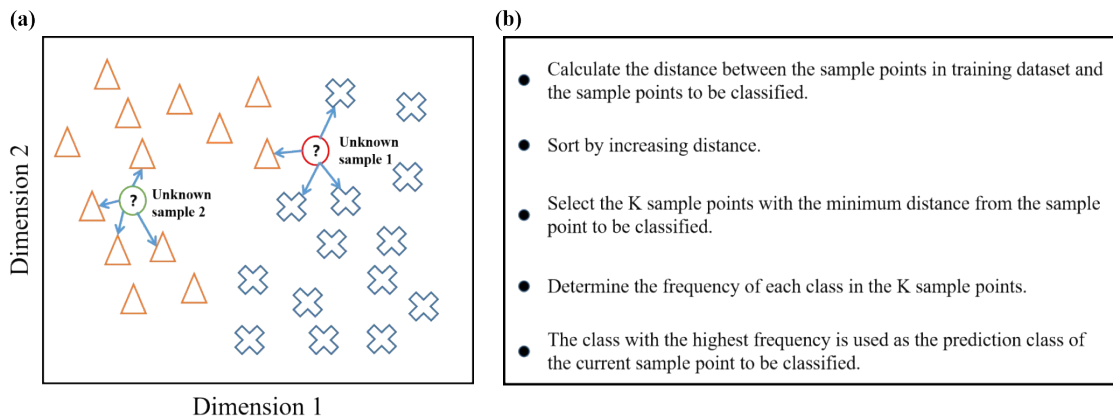


Fig. S3. A typical workflow for KNN algorithm. (a) Predict the class for the unknown sample 1 and the unknown sample 2 via four nearest neighbours algorithms. (b) The pseudo code for the KNN algorithm.

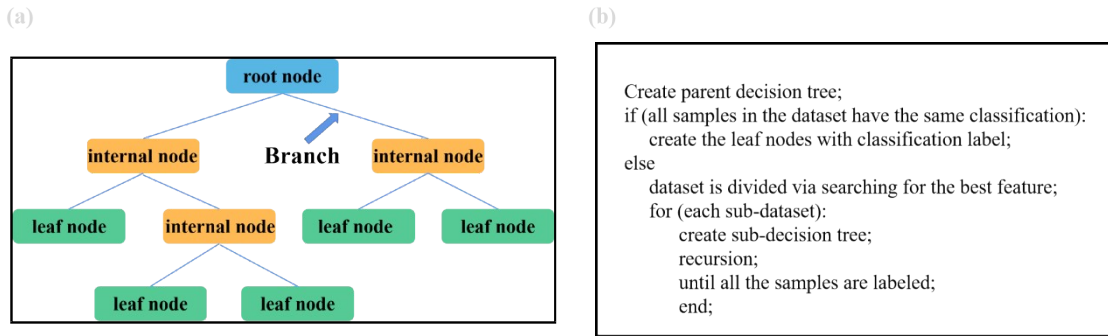


Fig. S4. The simple architecture and pseudo code of DT. (a) The simple architecture of DT consists of 1 root node, 8 branches, 3 internal nodes, and 4 leaf nodes. (b) The pseudo code for the DT algorithm.

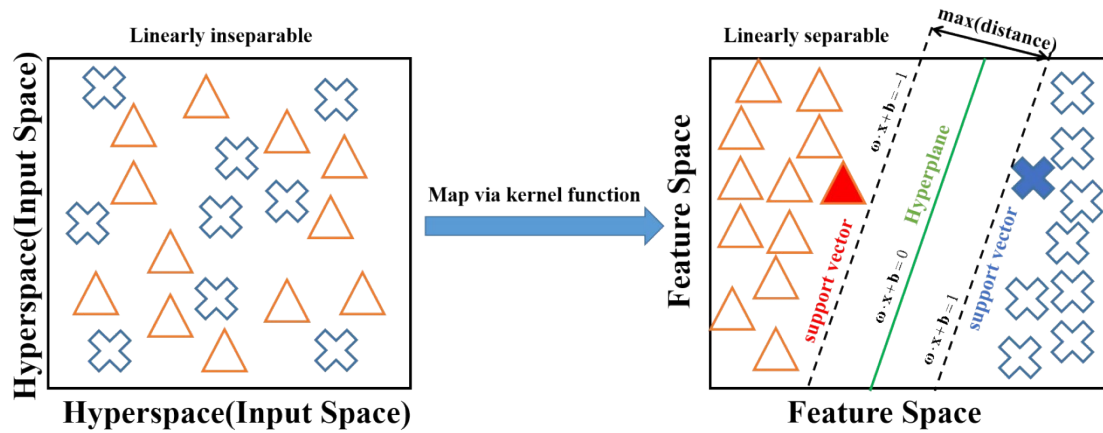


Fig. S5. A general flow to solve a classification problem with high dimension using SVM.

Transform the problem with linear inseparability to the problem with linear separability via kernel function.

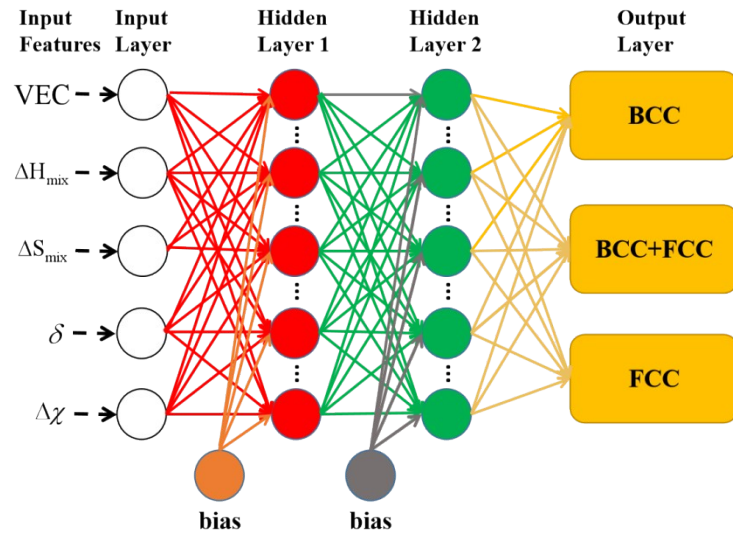


Fig. S6. Fully-connected ANN structure for phase prediction. A typical architecture of ANN consisting of an input layer, two hidden layers, and one output layer.

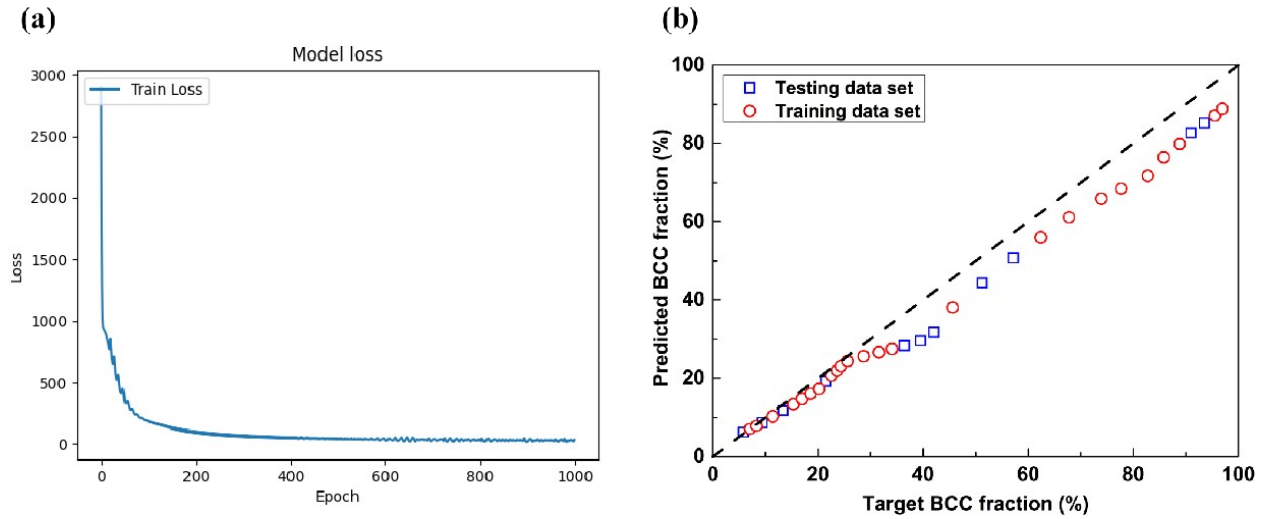


Fig. S7. Performance evaluation of the ANN model for the phase fraction prediction. (a) The performance curve of the ANN model. (b) The prediction results of a training data set test data set based on the ANN model.

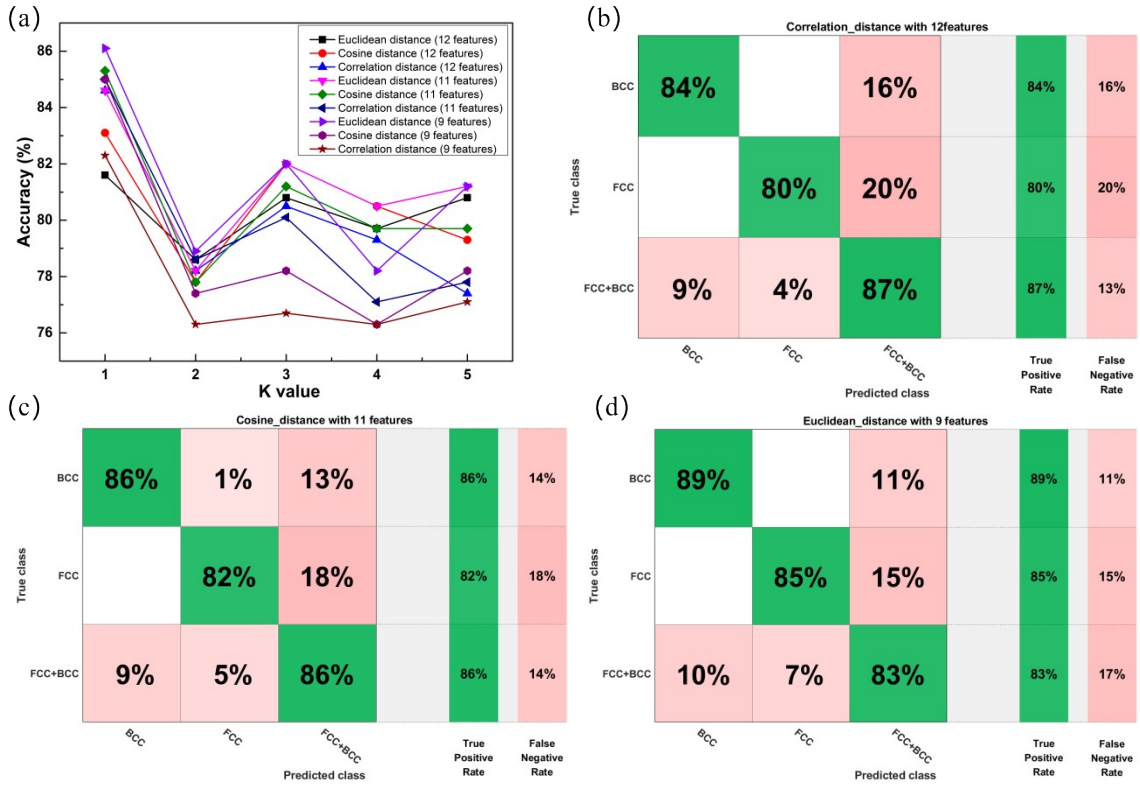


Fig. S8. Performance evaluation of the KNN algorithm. (a) The effect of the distance metric and K value on the prediction accuracy of the KNN algorithm with twelve/eleven/nine features. (b-d) The classification result in the form of a confusion matrix using the KNN algorithm with correlation, cosine, and Euclidean, distances, respectively.

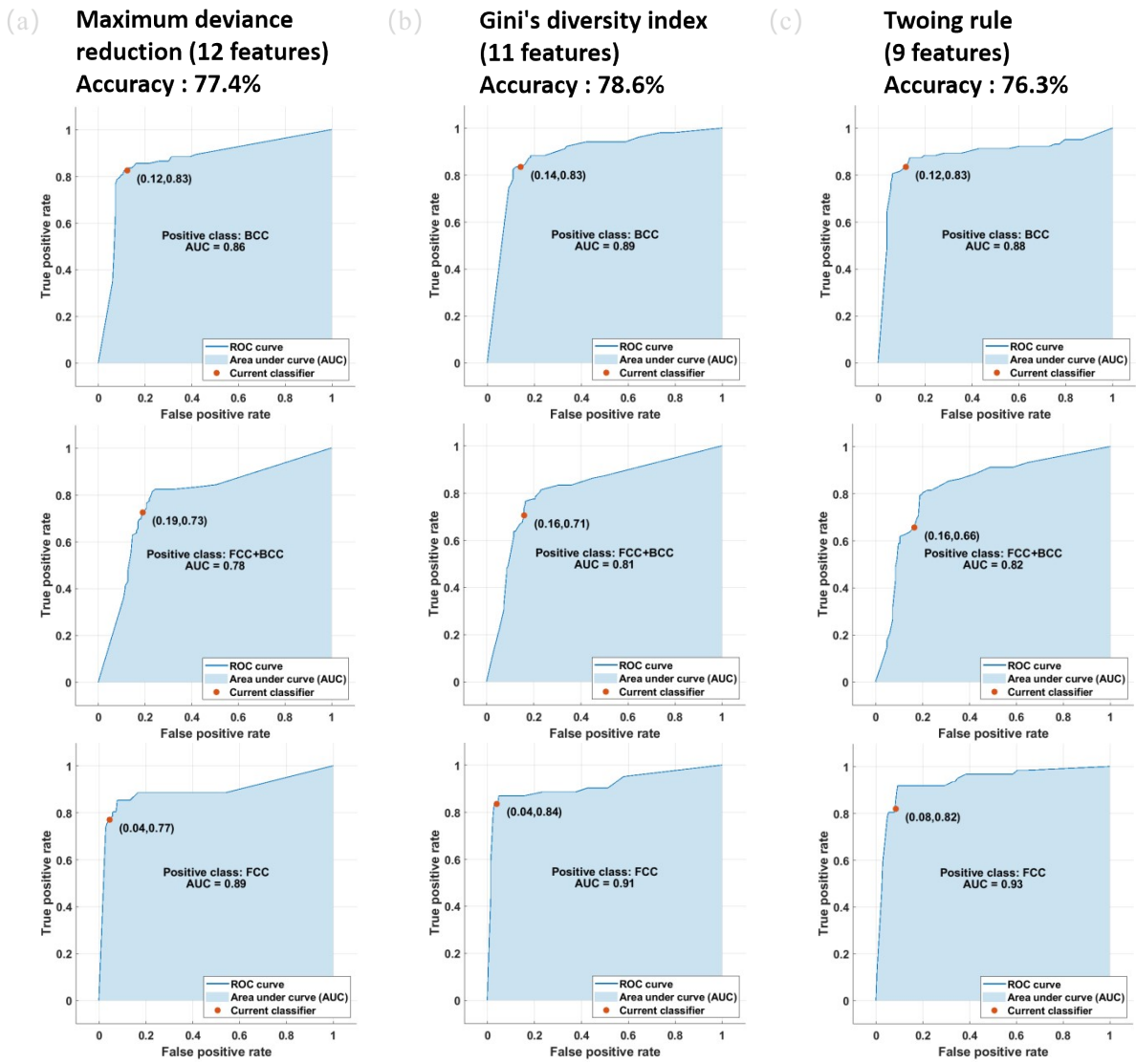


Fig. S9. Performance evaluation of the DT algorithm. (a-c) Evaluating the prediction accuracy of the DT algorithm with 12 features, 11 features, and 9 features, under the condition of different split criteria in the form of the ROC curve

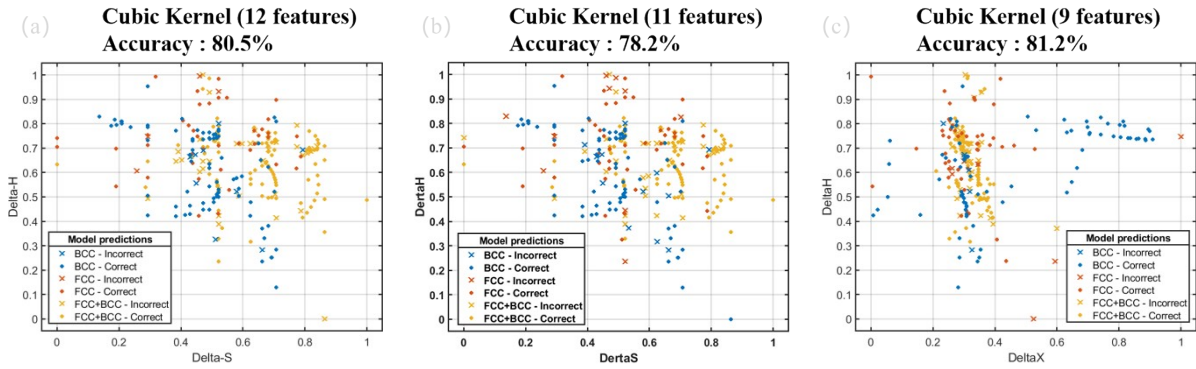


Fig. S10. Performance evaluation of the SVM algorithm. (a-c) The classification results for the phase selection of MPEAs with 12, 11, and 9 features, via the Cubic kernel SVM algorithm.

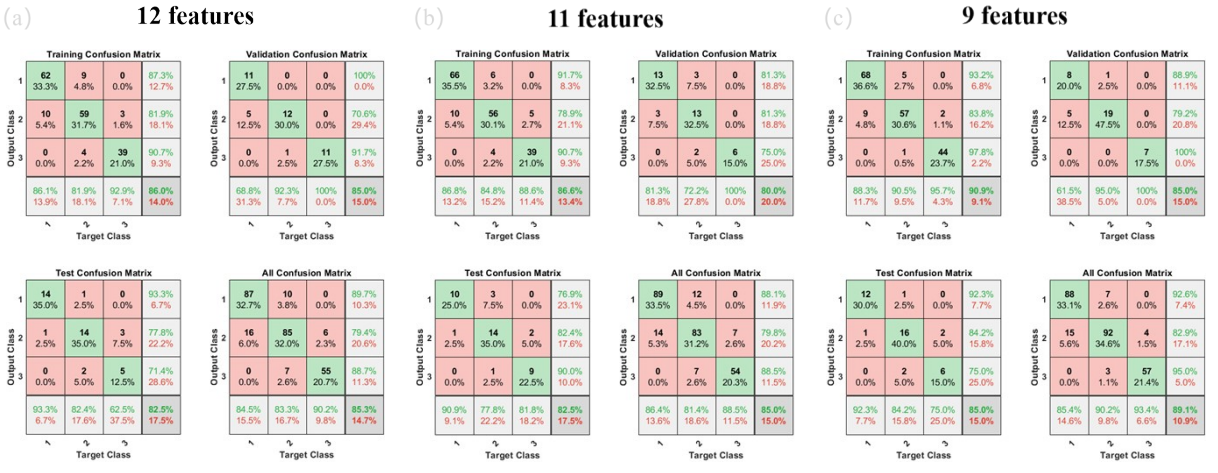


Fig. S11. Performance evaluation of the ANN algorithm. (a-c) The classification result in the training data set, validation data set, test data set and all data, using the ANN algorithm with 12 features, 11 features, and 9 features, respectively. Here, “1” represents BCC structure; “2” represents the BCC + FCC phase; “3” denotes the FCC phase.

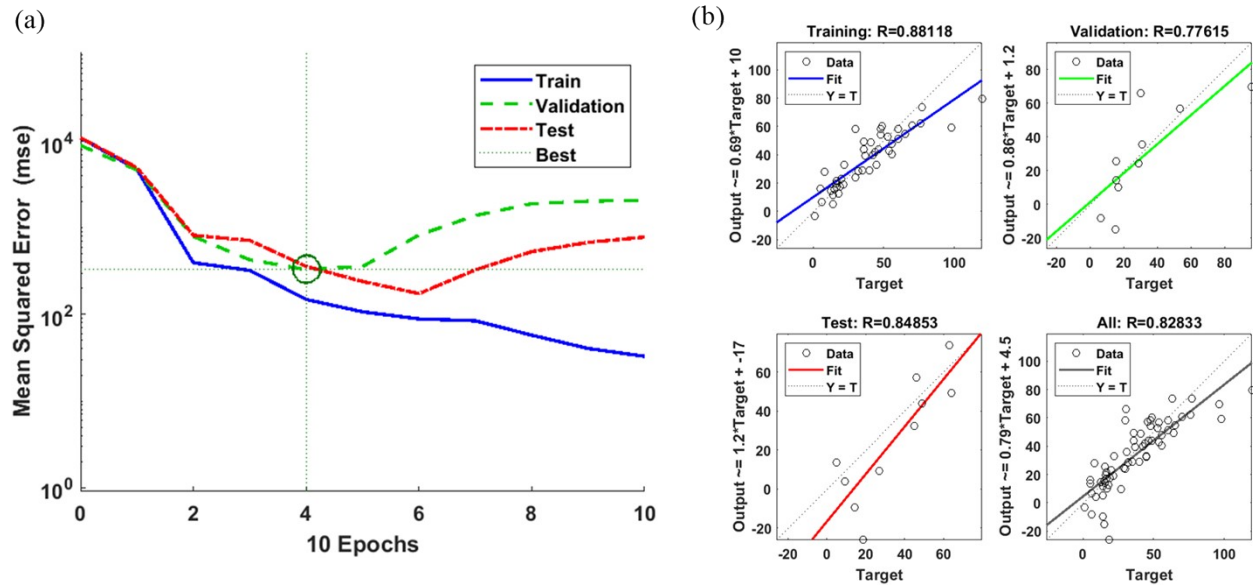


Fig. S12. Performance evaluation of the machine learning model for the elongation prediction. (a) The performance curve of the ANN model. (b) The prediction results of a training data set, validation data set, test data set, and all data based on the ANN model.

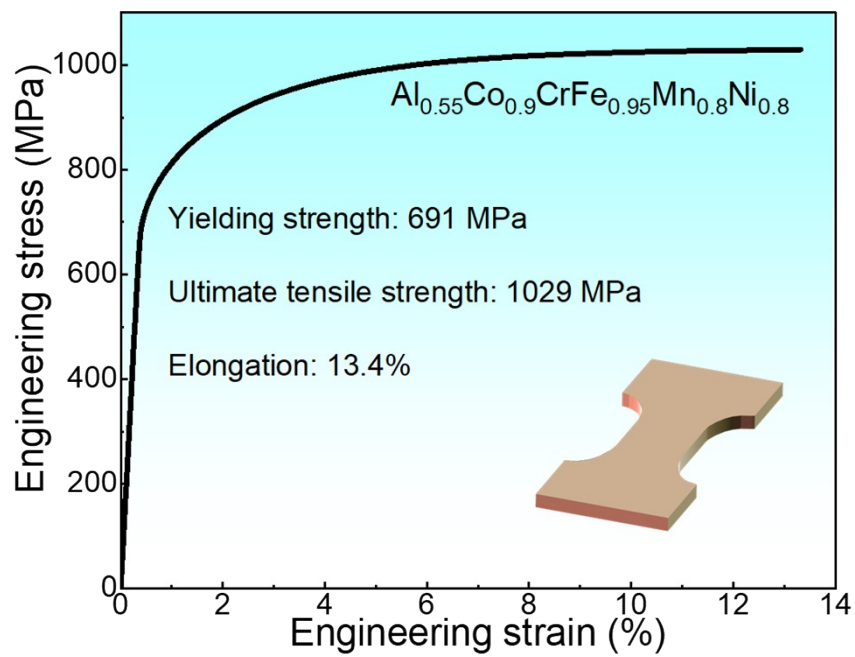


Fig. S13. Tensile stress-strain curve of the $\text{Al}_{0.55}\text{Co}_{0.9}\text{CrFe}_{0.95}\text{Mn}_{0.8}\text{Ni}_{0.8}$.

Table S1. The description and formula of initial physical features.

Abbreviation	Formula	Description
ΔS_{mix}	$\Delta S_{\text{mix}} = -R \sum_{i=1}^n c_i \ln c_i$	Mixing Entropy ¹³
ΔH_{mix}	$\Delta H_{\text{mix}} = 4 \sum_{i=1, i \neq j}^n c_i c_j H_{ij}^m$	Mixing Enthalpy ¹³
T_m	$T_m = \sum_{i=1}^n x_i (T_m)_i$	Average melting temperature ¹⁴
Ω	$\Omega = \frac{T_m \Delta S_{\text{mix}}}{ H_{\text{mix}} }$	The stability ¹⁴
$\Delta \chi$	$\Delta \chi = \sqrt{\sum_{i=1}^n c_i \left(1 - \frac{\chi_i}{\bar{\chi}}\right)^2}$	Electronegativity Mismatch ¹³
δr	$\delta r = \sqrt{\sum_{i=1}^n c_i \left(1 - \frac{r_i}{\bar{r}}\right)^2}$	Atomic-Size Mismatch ¹³
VEC	$VEC = \sum_{i=1}^n c_i VEC_i$	Valence Electron Concentration ¹⁵
γ	$\gamma = \left(1 - \sqrt{\frac{(r + r_{\min})^2 - r^2}{(r + r_{\min})^2}}\right) / \left(1 - \sqrt{\frac{(r + r_{\max})^2 - r^2}{(r + r_{\max})^2}}\right)$	γ parameter ¹⁶
E	$E = \sum_{i=1}^n c_i E_i$	Young's Modulus
B	$B = \sum_{i=1}^n c_i B_i$	Bulk Modulus
ρ	$\rho = \sum_{i=1}^n c_i \rho_i$	Density
λ	$\lambda = \frac{\Delta S_{\text{mix}}}{\delta^2}$	A geometrical parameter ¹⁷

Table S2. Data source of the prediction accuracy comparisons between different models.

MPEAs	Experimental yield strength (MPa)	Classical solid-solution model ¹⁸	Senkov's model ¹⁹	Toda-Caraballo's model ²⁰	Our model (MPa)
CrCoFeNiMn ²¹	214	452	260	373	205
TiNbTaZrHf ²¹	876	1,653	1,094	331	850
Al _{0.5} CrCoFeNiMn ²¹	357	589	493	472	381
Average deviation (%)		88.1	28.1	56.2	4.6
Average accuracy (%)		11.9	71.9	43.8	95.4

Table S3. Chemical compositions of the Al_{0.63}Co_{0.95}Cr_{0.95}FeMn_{0.74}Ni alloy constituents in the as-cast condition, in atomic percent (at.%).

The data derived by the TEM-based EDS.

Constituent	Al	Co	Cr	Fe	Ni	Mn
FCC	13.7	16.3	20.5	20.6	15.8	13.1
B2	35.8	13.4	4.7	7.1	26.0	13.0
BCC	9.3	13.4	37.9	24.7	5.9	8.8
Alloy composition	11.3	18.3	18.1	19.6	19.2	13.5

Table S4. Detailed information about the data sources for Fig. 5E.

	Alloys	Yield Strength (MPa)	Elongation (%)
System and Subsystem:			
	Al0.56CoCrFeMnNi ¹²	526	16
	Al0.62CoCrFeMnNi ¹²	833	5
	Al0.67CoCrNiFe1.94 ²²	866	7.9
	AlCoCrFeNi2.15 ²³	545	16.5
	CoCr0.38Fe0.15Ni0.15 ²⁴	482	13.3
	CrFeNi2.1Al0.9 ²⁵	610	9.1
	CrFeNi2.2Al0.8 ²⁵	479	12.7
	CrFeNi2Al ²⁵	774	6.4
	Al0.14Cr0.34FeMn0.8Ni0.57 ²⁶	1,253	6.78
Other MPEAs	FeCrCuMnNi ²⁷	628	14.5
	CoCrFeNi2.1Nb0.4 ²⁸	640	7
	CoCuFeMnNiSn0.05 ²⁹	475	12
	CoCuFeNiSn0.1 ³⁰	602	5
	NbTaTi ³¹	620	18.5

Table S5. Detailed information about data sources for Fig. 6.

	Exp.		Model + Exp.		High-throughput + Exp.		Simul. + Exp.		Machine learning+ Exp.		Our work	
	C	E	C	E	C	E	C	E	C	E	C	E
MPEAs ^{32, 33}	180	300	6	100	95	31	25	38	12	15	2	2
Superalloys ³⁴	120	350	11	210	130	61	35	65	11	19	-	-
Mg-alloys ^{35, 36}	150	200	8	90	80	50	37	110	9	7	-	-
Stainless steel ³⁷	92	200	7	190	58	25	25	110	18	7	-	-
Al-alloys ^{35, 38}	70	280	12	110	52	40	25	39	8	11	-	-

C represents cost (pieces); E denotes efficiency (days)

Table S6. Optimal composition. The predicted yield strengths and elongations of candidate MPEAs as well as the corresponding compositions and volume fractions of the FCC/BCC structures.

Al (at. %)	Fe (at. %)	Co (at. %)	Cr (at. %)	Ni (at. %)	Mn (at. %)	BCC (%)	FCC (%)	Elongation (%)	Yield Strength (MPa)
12.00	19.08	18.07	18.35	18.80	13.7	29.50	70.50	13.28	833.80
11.00	17.57	19.57	19.24	16.06	16.56	22.46	77.54	15.38	740.15
10.00	19.59	17.55	16.43	17.88	18.55	18.44	81.56	18.81	663.61
10.00	19.89	18.94	18.99	16.94	15.24	14.85	85.15	18.87	646.38
10.00	16.91	17.07	19.94	18.95	17.13	17.33	82.67	19.44	651.60
10.00	18.80	19.14	17.09	18.26	16.70	14.58	85.42	19.68	647.57
10.00	19.52	17.36	16.38	16.86	19.87	20.41	79.59	18.12	673.73
10.00	18.58	17.80	16.30	17.66	19.65	19.52	80.48	18.79	669.24
9.00	16.55	19.94	16.89	16.34	21.27	12.05	87.95	22.86	582.40
10.00	17.37	16.85	19.08	17.60	19.09	20.20	79.80	18.26	667.51
10.00	19.65	19.42	19.00	16.03	15.90	15.35	84.65	18.51	649.26
10.00	16.54	19.26	18.09	18.33	17.79	15.38	84.62	20.00	649.77
10.00	16.69	16.09	19.01	17.00	21.21	23.98	76.02	17.67	688.23
10.00	16.17	16.57	18.05	17.85	21.36	23.13	76.87	18.52	686.04
10.00	16.65	19.61	16.62	18.00	19.11	16.65	83.35	19.94	658.91
11.00	18.16	16.72	16.74	19.58	17.80	24.57	75.43	16.14	750.28
11.00	18.48	17.32	18.79	18.26	16.15	22.97	77.03	15.62	739.46
11.00	18.32	17.82	19.23	18.28	15.35	21.68	78.32	15.90	733.43
10.00	17.05	17.48	17.89	16.03	21.55	22.71	77.29	17.71	686.09
11.00	18.52	17.89	16.16	18.80	17.64	23.41	76.59	16.15	747.37
10.00	16.65	18.48	18.60	16.25	20.03	19.66	80.34	18.27	669.98
11.00	19.31	19.34	19.75	17.42	13.18	18.80	81.20	16.30	724.06
11.00	18.41	19.09	19.31	17.62	14.56	20.08	79.92	16.09	728.67
10.00	16.67	19.80	16.53	16.47	20.54	18.43	81.57	19.22	669.54
11.00	16.46	18.32	18.10	19.47	16.65	21.36	78.64	16.81	735.78
11.00	17.14	16.75	15.82	18.93	20.35	28.52	71.48	15.85	771.88
11.00	17.04	16.28	17.02	18.31	20.35	29.19	70.81	15.26	773.29
11.00	15.81	17.59	17.76	19.63	18.21	24.03	75.97	16.63	748.66
11.00	18.98	16.80	15.95	16.69	20.57	28.72	71.28	14.63	773.84
11.00	17.01	19.12	15.90	19.06	17.92	22.33	77.67	16.90	745.38
12.00	19.45	15.90	17.93	19.02	15.70	40.78	59.22	12.53	879.29
11.00	17.91	17.65	19.20	15.97	18.27	26.39	73.61	14.45	755.99
11.00	16.99	19.58	17.42	17.89	17.12	21.56	78.44	16.35	740.00
11.00	18.89	19.01	16.85	16.07	18.19	24.27	75.73	15.13	752.92
12.00	19.13	16.87	18.22	19.25	14.53	34.57	65.43	13.02	853.50
11.00	18.12	19.77	15.83	17.26	18.02	22.72	77.28	16.10	748.45
11.00	16.03	16.63	18.13	17.45	20.75	29.70	70.30	14.89	776.51
12.00	18.94	15.65	16.63	18.94	17.83	43.57	56.43	12.28	894.89

12.00	19.21	15.97	19.07	17.74	16.01	44.26	55.74	11.94	890.53
11.00	18.19	18.49	17.07	15.85	19.41	26.23	73.77	14.81	761.69
12.00	19.08	17.27	17.48	18.68	15.49	34.56	65.44	12.77	855.39
11.00	16.64	19.72	17.66	17.23	17.75	22.56	77.44	16.06	744.78
12.00	19.52	19.52	17.44	18.81	12.71	23.44	76.56	13.88	815.30
12.00	18.81	19.14	15.87	19.56	14.61	24.80	75.20	13.86	822.17
12.00	17.74	18.53	19.58	19.44	12.71	26.81	73.19	14.01	820.11
12.00	18.21	19.34	16.62	19.52	14.32	24.39	75.61	14.01	818.78
12.00	18.12	16.01	17.36	18.13	18.38	45.24	54.76	11.98	901.27
12.00	18.98	16.55	15.73	17.30	19.45	39.52	60.48	11.88	882.47
12.00	18.58	17.24	17.40	16.73	18.06	40.41	59.59	11.80	881.49
12.00	19.12	16.37	16.74	16.05	19.72	42.60	57.40	11.25	894.77
12.00	16.79	16.89	18.16	17.91	18.24	43.05	56.95	12.14	891.86
12.00	18.13	15.78	17.52	15.85	20.72	48.38	51.62	10.93	920.23
12.00	17.65	17.77	19.44	15.84	17.29	41.39	58.61	11.59	880.99
12.00	17.30	19.60	17.86	16.80	16.45	29.80	70.20	12.75	838.32
12.00	17.67	16.68	17.99	15.69	19.97	46.95	53.05	11.13	911.96
12.00	18.19	18.03	15.82	15.89	20.07	35.61	64.39	11.77	869.74
13.00	18.59	19.34	19.24	18.90	10.93	46.87	53.13	11.29	976.79
12.00	16.99	19.01	18.29	16.01	17.71	34.60	65.40	12.15	858.07
12.00	17.23	16.00	15.70	15.74	23.34	41.23	58.77	11.14	903.97
13.00	17.87	17.13	19.31	18.77	13.92	60.92	39.08	10.10	1029.14
13.00	18.32	15.94	16.84	18.30	17.59	72.94	27.06	9.24	1087.96
13.00	19.09	16.36	18.17	16.24	17.14	73.09	26.91	8.73	1082.99
13.00	18.77	19.06	16.03	16.69	16.45	63.87	36.13	9.70	1052.86
13.00	15.84	17.39	16.69	19.15	17.93	67.98	32.02	9.98	1074.23
13.00	16.00	16.87	18.47	18.17	17.49	71.25	28.75	9.48	1080.78
13.00	17.56	18.76	15.50	17.25	17.94	65.99	34.01	9.75	1065.07
13.00	18.22	18.24	15.97	15.99	18.58	68.55	31.45	9.15	1074.41
13.00	16.50	17.45	16.49	16.64	19.92	72.76	27.24	9.05	1096.68

Table S7. Predicted results versus Experimental results. The comparison between the properties of predictions and those of experiments in the Al_{0.63}Co_{0.95}Cr_{0.95}FeMn_{0.74}Ni MPEA

MPEA composition	Predictive results				Experimental results			
	BCC (%)	FCC (%)	YS (MPa)	EL (%)	BCC (%)	FCC (%)	YS (MPa)	EL (%)
Al_{0.63}Co_{0.95}Cr_{0.95}FeMn_{0.74}Ni	29.69	70.31	954	13.4	28	72	880	12.3

Table S8. Predicted results versus Experimental results. The comparison between the properties of predictions and experiments of $\text{Al}_{0.55}\text{Co}_{0.9}\text{CrFe}0.95\text{Mn}_{0.8}\text{Ni}_{0.8}$ MPEA.

MPEA composition	Predictive results		Experimental results	
	YS (MPa)	EL (%)	YS (MPa)	EL (%)
$\text{Al}_{0.55}\text{Co}_{0.9}\text{CrFe}0.95\text{Mn}_{0.8}\text{Ni}_{0.8}$	730	14.5	691	13.4

Data S1. The initial data collected from the experiments (separate file)

The initial data set includes 325 entries derived from the experiments in the prior research, including alloy compositions, phase structures and references.

Alloys	Phases	Reference
CoFeNi	FCC	T.T. Zuo, R.B. Li, X.J. Ren, Y. Zhang, Effects of Al and Si addition on the structure and properties of CoFeNi equal atomic ratio alloy, <i>J. Magn. Magn. Mater.</i> 371 (2014) 60–68.
CoFeNiSi0.25	FCC	
Al0.25CoFeNi	FCC	
Al0.5CoFeNi	FCC+BCC	
Al0.75CoFeNi	FCC+BCC	
AlCoFeNi	BCC	
CoFeNi	FCC	Z. Wu, H. Bei, G.M. Pharr, E.P. George, Temperature dependence of the mechanical properties of equiatomic solid solution alloys with face-centered cubic crystal structures, <i>Acta Mater.</i> 81 (2014) 428–441.
CoCrNi	FCC	
CoMnNi	FCC	
FeMnNi	FCC	
CoCrFeNi	FCC	
CoCrMnNi	FCC	
CoFeMnNi	FCC	Y.F. Kao, T.J. Chen, S.K. Chen, J.W. Yeh, Microstructure and mechanical property of as-cast, -homogenized, and -deformed Al _x CoCrFeNi high entropy alloys, <i>J. Alloy. Compd.</i> 488 (2009) 57–64.
CoCrFeNi	FCC	
CoCrFeNi	FCC	
Al0.25CoCrFeNi	FCC	
Al0.25CoCrFeNi	FCC	
Al0.375CoCrFeNi	FCC	
Al0.375CoCrFeNi	FCC	
Al0.5CoCrFeNi	FCC+BCC	
Al0.5CoCrFeNi	FCC+BCC	
Al0.75CoCrFeNi	FCC+BCC	
Al0.75CoCrFeNi	FCC+BCC	
Al0.875CoCrFeNi	BCC	
Al0.875CoCrFeNi	FCC+BCC	
AlCoCrFeNi	BCC	
AlCoCrFeNi	FCC+BCC	
Al1.25CoCrFeNi	BCC	
Al1.25CoCrFeNi	BCC	
Al1.5CoCrFeNi	BCC	
Al1.5CoCrFeNi	BCC	
Al2CoCrFeNi	BCC	
Al2CoCrFeNi	BCC	

Al2CoCrFeMo0.5Ni	BCC	C.-Y. Hsu, C.-C. Juan, T.-S. Sheu, S.-K. Chen, J.-W. Yeh, Effect of aluminum content on microstructure and mechanical properties of AlxCoCrFeMo0.5Ni high-entropy alloys, <i>JOM</i> 65 (2013) 1840–1847.
CoCrFeNiTi	FCC	K.B. Zhang, Z.Y. Fu, J.Y. Zhang, W.M. Wang, H. Wang, Y.C. Wang, Q.J. Zhang, J. Shi, Microstructure and mechanical properties of CoCrFeNiTiAlx high entropy alloys, <i>Mater. Sci. Eng. A</i> 508 (2009) 214–219.
Al1.5CoCrFeNiTi	BCC	
Al2CoCrFeNiTi	BCC	
Co1.5CrFeNi1.5Ti0.5	FCC	
Al0.2Co1.5CrFeNi1.5Ti0.5	FCC	M.-H. Chuang, M.-H. Tsai, W.-R. Wang, S.-J. Lin, J.-W. Yeh, Microstructure and wear behavior of AlxCo1.5CrFeNi1.5Ti0.5 high entropy alloys, <i>Acta Mater.</i> 59 (2011) 6308–6317.
Al0.7Co0.3CrFeNi	FCC+BCC	Weiping Chen, Zhiqiang Fu, Sicong Fang, Huaqiang Xiao, Dezhi Zhu, Alloying behavior, microstructure and mechanical properties in a FeNiCrCo0.3Al0.7 high entropy alloy, <i>Mater. Des.</i> 51 (2013) 854–860.
Al0.875CoCrFeNi	FCC+BCC	B.S. Murty, J. Yeh, S. Ranganathan, High Entropy Alloys, 1st edition, Butterworth-Heinemann, ISBN 9780128002513.
AlCoCrFeNi	BCC	
Al1.5CoCrFeNi	BCC	
Al2CoCrFeNi	BCC	
Al2.5CoCrFeNi	BCC	
Al3CoCrFeNi	BCC	
CoCrCuFeNi	FCC	
CrCuFeMnNi	FCC+BCC	
CrCuFeMoNi	FCC	
AlCrCuFeNi	FCC+BCC	
AlCoCrFeNi	BCC	Y.P. Wang, B.S. Li, M.X. Ren, C. Yang, H.Z. Fu, Microstructure and compressive properties of AlCrFeCoNi high entropy alloy, <i>Mater. Sci. Eng. A</i> 491 (2008) 154–158.
AlCoCrFeMo0.1Ni	BCC	J.M. Zhu, H.M. Fu, H.F. Zhang, A.M. Wang, H. Li, Z.Q. Hua, Microstructures and compressive properties of multicomponent AlCoCrFeNiMox alloys, <i>Mater. Sci. Eng. A</i> 527 (2010) 6975–6979.
AlCoCrFeNb0.1Ni	BCC	S.G. Ma, Y. Zhang, Effect of Nb addition on the microstructure and properties of AlCoCrFeNi high-entropy alloy, <i>Mater. Sci. Eng. A</i> 532 (2012) 480–486.
AlCo2CrFeMo0.5Ni	FCC+BCC	C.-Y. Hsu, W.-R. Wang, W.-Y. Tang, S.-K. Chen, J.-W. Yeh, Microstructure and mechanical properties of

		new Al _x CrFeMo0.5Ni high-entropy alloys, <i>Adv. Eng. Mater.</i> 12 (2010) 44–49.
AlCoCrFeMo0.5Ni1.5	FCC+BCC	C.-C. Juan, C.-Y. Hsu, C.-W. Tsai, W.-R. Wang, T.-S. Sheu, J.-W. Yeh, S.-K. Chen, On microstructure and mechanical performance of AlCoCrFeMo0.5Ni _x high-entropy alloys, <i>Intermetallics</i> 32 (2013) 401–407.
AlCoCrFeMo0.5Ni2	FCC+BCC	J.M. Zhu, H.M. Fu, H.F. Zhang, A.M. Wang, H. Li, Z.Q. Hu, Synthesis and properties of multiprincipal component AlCoCrFeNiSix alloys, <i>Mater. Sci. Eng. A</i> 527 (2010) 7210–7214.
AlCoCrFeNiSi0.2	BCC	
AlCoCrFeNiSi0.4	BCC	
AlCoCrFeNiSi0.6	BCC	
AlCoCrFeNiSi	BCC	
AlCoCrFeNiTi0.5	FCC	
CoCrCuFeNiTi0.5	FCC	
Al0.25CoCrCu0.5FeNiTi0.5	FCC	
Al0.25CoCrCu0.75FeNiTi0.5	FCC	
Al0.5CoCrCu0.5FeNiTi0.5	FCC+BCC	
Al0.75CoCrCu0.25FeNiTi0.5	FCC+BCC	
AlCoCrFeNiTi0.5	BCC	
AlCoCrFeNiTi	BCC	
AlCoFeNiTiVZr	BCC	J.-W. Yeh, S.-K. Chen, S.-J. Lin, J.-Y. Gan, T.-S. Chin, T.-T. Shun, C.-H. Tsau, S.-Y. Chang, Nanostructured high-entropy alloys with multiple principal elements: novel alloy design concepts and outcomes, <i>Adv. Eng. Mater.</i> 6 (2004) 299–303.
CoCrFeMnNi	FCC	
Al0.10CoCrFeMnNi	FCC	
Al0.20CoCrFeMnNi	FCC	
Al0.38CoCrFeMnNi	FCC	
Al0.43CoCrFeMnNi	FCC+BCC	
Al0.49CoCrFeMnNi	FCC+BCC	
Al0.56CoCrFeMnNi	FCC+BCC	
Al0.62CoCrFeMnNi	FCC+BCC	
Al0.68CoCrFeMnNi	FCC+BCC	
Al0.75CoCrFeMnNi	FCC+BCC	
Al0.81CoCrFeMnNi	FCC+BCC	
Al0.88CoCrFeMnNi	FCC+BCC	
Al0.95CoCrFeMnNi	FCC+BCC	
Al1.25CoCrFeMnNi	BCC	
CoCrFeMnNi	FCC	
CoCrFeMnNiV0.25	FCC	
CoCrFeMnNiV0.5	FCC	N.D. Stepanov, D.G. Shaysultanov, G.A. Salishchev, M.A. Tikhonovsky, E.E. Oleynik, A.S. Tortika, O.N. Senkov, Effect of V content on microstructure and mechanical properties of the CoCrFeMnNiV _x high entropy alloys, <i>J. Alloy.</i>

		Compd. 628 (2015) 170–185.
Al0.5CrFe1.5MnNi0.5	BCC	S.T. Chen, et al., Microstructure and properties of age-hardenable AlxCr-Fe1.5MnNi0.5 alloys, Mater. Sci. Eng. A 527 (2010) 5818–5825.
Al0.3CrFe1.5MnNi0.5	FCC+BCC	
AlCrFeNi	BCC	
AlCrFeNiMo0.2	BCC	
AlCrFeNiMo0.5	BCC	
Al0.3CoCrCuFe	FCC	
Al0.5CoCrCuFe	FCC	
Al0.8CoCrCuFe	FCC+BCC	
AlCoCrCuFe	FCC+BCC	
Al1.3CoCrCuFe	FCC+BCC	
Al1.5CoCrCuFe	FCC+BCC	
Al1.8CoCrCuFe	FCC+BCC	
Al2.0CoCrCuFe	FCC+BCC	
Al2.3CoCrCuFe	FCC+BCC	
Al2.5CoCrCuFe	FCC+BCC	
Al2.8CoCrCuFe	BCC	
Al3.0CoCrCuFe	BCC	
CoCrCu0.5FeNi	FCC	Jien-Wei Yeh, Recent Progress in High-entropy Alloys, Ann. De. Chim. – Sci. Des. Mater. 31 (2006) 633–648. Chun-Ming Lin, Hsien-Lung Tsai, Hui-Yun Bor, Effect of aging treatment on microstructure and properties of high-entropy Cu0.5CoCrFeNi alloy, Intermetallics 18 (2010) 1244–1250.
CoCrCuFeNi	FCC	
Al0.3CoCrCuFeNi	FCC	
Al0.5CoCrCuFeNi	FCC	
Al0.8CoCrCuFeNi	FCC	
AlCoCrCuFeNi	FCC+BCC	
Al1.3CoCrCuFeNi	FCC+BCC	
Al1.5CoCrCuFeNi	FCC+BCC	
Al1.8CoCrCuFeNi	FCC+BCC	
Al2CoCrCuFeNi	FCC+BCC	
Al2.3CoCrCuFeNi	FCC+BCC	
Al2.5CoCrCuFeNi	FCC+BCC	
Al2.8CoCrCuFeNi	BCC	
CoCrCuFeNiTi0.5	FCC	X.F. Wang, Y. Zhang, Y. Qiao, G.L. Chen, Novel microstructure and properties of multicomponent CoCrCuFeNiTix alloys, Intermetallics 15 (2007) 357–362.
CoCrCuFeNiTi	FCC	
Al0.5CoCrCuFeNi	FCC	M.-R. Chen, S.-J. Lin, J.-W. Yeh, S.-K. Chen, Y.-S. Huang, C.-P. Tu, Microstructure and properties of Al0.5CoCrCuFeNiTix ($\chi_{\text{Co}} = 0.20$) high-entropy alloys, Mater. Trans. 47
Al0.5CoCrCuFeNiTi0.2	FCC	
Al0.5CoCrCuFeNiTi0.4	FCC	

Al0.5CoCrCuFeNiTi0.6	FCC+BCC	(2006) 1395–1401.
Al0.5CoCrCuFeNiTi0.8	FCC+BCC	
Al0.5CoCrCuFeNiTi	FCC+BCC	
Al0.5CoCrCuFeNiTi1.2	FCC+BCC	
Al0.5CoCrCuFeNiTi1.4	FCC+BCC	
Al0.5CoCrCuFeNiTi1.6	FCC+BCC	
Al0.5CoCrCuFeNiTi1.8	FCC+BCC	
Al0.5CoCrCuFeNiTi2	FCC+BCC	
Al0.5CoCrCuFeNi	FCC	
Al0.5CoCrCuFeNiV0.2	FCC	
Al0.5CoCrCuFeNiV0.4	FCC+BCC	M.R. Chen, S.J. Lin, J.W. Yeh, S.K. Chen, Y.S. Huang, M.H. Chuang, Effect of vanadium addition on the microstructure, hardness, and wear resistance of Al0.5CoCrCuFeNi high-entropy alloy, Metall. Mater. Trans. A 37A (2006) 1363–1369.
Al0.5CoCrCuFeNiV0.6	FCC+BCC	
Al0.5CoCrCuFeNiV0.8	FCC+BCC	
Al0.5CoCrCuFeNiV1.0	FCC+BCC	
Al0.5CoCrCuFeNiV1.2	BCC	
Al0.5CoCrCuFeNiV1.4	BCC	
Al0.5CoCrCuFeNiV1.6	BCC	
Al0.5CoCrCuFeNiV1.8	BCC	
Al0.5CoCrCuFeNiV2.0	BCC	
AlCoCrCuFeNi	FCC+BCC	
AlCoCuFeNi	FCC+BCC	
AlCoCuFeNiSi	FCC+BCC	
AlCoCuFeNiTi	FCC+BCC	
AlCoCuFeNiZr	FCC+BCC	
AlCoCrCuFeNi	FCC+BCC	
AlCoCrCuFeMnNi	FCC+BCC	
AlCoCrCuFeNiTi	FCC+BCC	
AlCoCrCuFeNiV	FCC+BCC	
Al3CoCrCuFeNi	BCC	J.-W. Yeh, Recent progress in high-entropy alloys, Ann. Chim. Sci. Mater. 31 (2006) 633–648.
AlCoCrCuNiTi	BCC	Z. Hu, Y. Zhan, G. Zhang, J. She, C. Li, Effect of rare earth Y addition on the microstructure and mechanical properties of high entropy AlCoCrCuNiTi alloys, Mater. Des. 31 (2010) 1599–1605.
CoCuFeNi	FCC	L. Liu, J.B. Zhu, C. Zhang, J.C. Li, Q. Jiang, Microstructure and the properties of FeCoCuNiSn _x high entropy alloys, Mater. Sci. Eng. A 548 (2012) 64–68.
CoCuFeNiSn0.02	FCC	
CoCuFeMnNi	FCC	
CoCuFeMnNiSn0.03	FCC	
CoCrCuFeNi	FCC	P. Jinhong, P. Ye, Z. Hui, Z. Lu, Microstructure and

AlCrCuFeNi0.6	FCC+BCC	properties of AlCrFeCuNix (0.6 ¼ ¼ 1.4) high-entropy alloys, Mater. Sci. Eng. A 534 (2012) 228–233.
AlCrCuFeNi0.8	FCC+BCC	
AlCrCuFeNi	FCC+BCC	
AlCrCuFeNi1.2	FCC+BCC	
AlCrCuFeNi1.4	FCC+BCC	
AlCrCuFeNi2	FCC+BCC	S. Guo, C. Ng, J. Lu, C.T. Liu, Effect of valence electron concentration on stability of FCC or BCC phase in high entropy alloys, J. Appl. Phys. 109 (2011) 103505.
Al0.2CrCuFeNi2	FCC	
Al0.4CrCuFeNi2	FCC	
Al0.6CrCuFeNi2	FCC	
Al0.8CrCuFeNi2	FCC	
Al1.2CrCuFeNi2	FCC+BCC	E. Fazakas, V. Zadorozhnyy, D.V. Louzguine-Luzgin, Effect of iron content on the structure and mechanical properties of Al25Ti25Ni25Cu25 and (AlTi)60-xNi20Cu20Fex (x ¼ 15, 20) high-entropy alloys, Appl. Surf. Sci. 358 (2015) 549–555.
Al1.125CuFe0.75NiTi1.125	FCC	
AlCuFeNiTi	FCC	
AlCuNiTi	FCC	
AlCr0.5NbTiV	BCC	
AlNbTiV	BCC	N.D. Stepanov, N. Yu Yurchenko, D.V. Skibin, M.A. Tikhonovsky, G.A. Salishchev, Structure and mechanical properties of the AlCr _x NbTiV (x ¼ 0, 0.5, 1, 1.5) high entropy alloys, J. Alloy. Compd. 652 (2015) 266–280.
Al0.4Hf0.6NbTaTiZr	BCC	
AlMo0.5NbTa0.5TiZr	BCC	
Al0.3NbTa0.8Ti1.4V0.2Zr1.3	BCC	
Al0.5NbTa0.8Ti1.5V0.2Zr	BCC	
Al0.3NbTaTi1.4Zr1.3	BCC	O.N. Senkov, C. Woodward, D.B. Miracle, Microstructure and properties of aluminum-containing refractory high entropy alloys, JOM 66 (10) (2014) 2030–2042.
AlNb1.5Ta0.5Ti1.5Zr0.5	BCC	
Al0.3HfNbTaTiZr	BCC	
Al0.5HfNbTaTiZr	BCC	
Al0.75HfNbTaTiZr	BCC	
HfNbTaTiZr	BCC	C.-M. Lin, C.-C. Juan, C.-H. Chang, C.-W. Tsai, J.-W. Yeh, Effect of Al addition on mechanical properties and microstructure of refractory Al _x HfNbTaTiZr alloys, J. Alloy. Compd. 624 (2015) 100–107.
Al0.25MoNbTiV	BCC	
Al0.5MoNbTiV	BCC	
Al0.75MoNbTiV	BCC	
AlMoNbTiV	BCC	
MoNbTiV	BCC	S.Y. Chen, X. Yang, K.A. Dahmen, P.K. Liaw, Y. Zhang, Microstructures and crackling noise of Al _x NbTiMoV high entropy alloys, Entropy 16 (2014) 870–884.
Al0.25NbTaTiV	BCC	
Al0.5NbTaTiV	BCC	
AlNbTaTiV	BCC	
NbTaTiV	BCC	
AlNbTiV	BCC	N.D. Stepanov, D.G. Shaysultanov, G.A. Salishchev, M.A. Tikhonovsky, Structure and mechanical properties of a lightweight AlNbTiV high entropy alloy, Mater. Lett. 142 (2015) 153–155.

NbTiVZr	BCC	O.N. Senkov, V. Senkova, D.B. Miracle, C. Woodward, Mechanical properties of low-density, refractory multi-principal element alloys of the Cr-Nb-Ti-V-Zr system, Mater. Sci. Eng. A 565 (2013) 51–62.
NbTiV2Zr	BCC	
HfMo0.25NbTaTiZr	BCC	
HfMo0.5NbTaTiZr	BCC	
HfMo0.75NbTaTiZr	BCC	
HfMoNbTaTiZr	BCC	C.-C. Juan, K.-K. Tseng, W.-L. Hsu, M.-H. Tsai, C.-W. Tsai, C.-M. Lin, S.-K. Chen, S.-J. Lin, J.-W. Yeh, Solution strengthening of ductile refractory HfMoxNbTaTiZr high-entropy alloys, Mater. Lett. 175 (2016) 284–287.
HfNbTaTiZr	BCC	
HfMoNbTaTiZr	BCC	C.-C. Juan, M.-H. Tsai, C.-W. Tsai, C.-M. Lin, W.-R. Wang, C.-C. Yang, S.-K. Chen, S.-J. Lin, J.-W. Yeh, Enhanced mechanical properties of HfMoTaTiZr and HfMoNbTaTiZr refractory high-entropy alloys, Intermetallics. 62 (2015) 76–83.
HfMoNbZrTi	BCC	N.N. Guo, L. Wang, L.S. Luo, X.Z. Li, Y.Q. Su, J.J. Guo, H.Z. Fu, Microstructure and mechanical properties of refractory MoNbHfZrTi high-entropy alloy, Mater. Des. 81 (2015) 87–94.
HfNbTaZr	BCC	S. Maiti, W. Steurer, Structural-disorder and its effect on mechanical properties in single-phase TaNbHfZr high-entropy alloy, Acta Mater. 106 (2016) 87–97.
Hf0.5Nb0.5Ta0.5Ti1.5Zr	BCC	S. Sheikh, S. Shafeie, Q. Hu, J. Ahlstrom, C. Persson, J. Vesely, J. Zyka, U. Klement, S. Guo, Alloy design for intrinsically ductile refractory high-entropy alloys, J. Appl. Phys. 120 (2016) 164902.
Mo0.3NbTiVZr	BCC	
Mo0.5NbTiVZr	BCC	
Mo0.7NbTiVZr	BCC	
MoNbTiVZr	BCC	
Mo1.3NbTiVZr	BCC	
Mo1.5NbTiVZr	BCC	
Mo1.7NbTiVZr	BCC	
Mo2NbTiVZr	BCC	
NbTiV0.3Zr	BCC	
NbTiV0.3Mo0.1	BCC	Y.D. Wu, Y.H. Cai, X.H. Chen, T. Wang, J.J. Si, L. Wang, Y.D. Wang, X.D. Hui, Phase composition and solid solution strengthening effect in TiZrNbMoV high-entropy alloys, Mater. Des. 83 (2015) 651–660.
NbTiV0.3Mo0.3	BCC	
NbTiV0.3Mo0.5	BCC	
NbTiV0.3Mo0.7	BCC	
NbTiV0.3Mo	BCC	
NbTiV0.3Mo1.3	BCC	
NbTiV0.3Mo1.5	BCC	
NbTiVZr	BCC	

MoNbTiV0.25Zr	BCC	<p>Y. Zhang, X. Yang, P.K. Liaw, Alloy design and properties optimization of high entropy alloys, JOM 64 (7) (2012) 830–838.</p>
MoNbTiV0.50Zr	BCC	
MoNbTiV0.75Zr	BCC	
MoNbTiV1.0Zr	BCC	
MoNbTiV1.5Zr	BCC	
MoNbTiV2.0Zr	BCC	
MoNbTiV3.0Zr	BCC	
MoNbTiZr	BCC	
NbTaVW	BCC	H.W. Yao, J.W. Qiao, M.C. Gao, J.A. Hawk, S.G. Ma, H.F. Zhou, Y. Zhang, NbTaV-(Ti,W) refractory high-entropy alloys: experiments and modeling, Mater. Sci. Eng. A-Struct. Mater. Prop. Microstruct. Process. 674 (2016) 203–211.
CoFeNiV	FCC	L. Jiang, Z.Q. Cao, J.C. Jie, J.J. Zhang, Y.P. Lu, T.M. Wang, T.J. Li, Effect of Mo and Ni elements on microstructure evolution and mechanical properties of the CoFeNixVMoy high entropy alloys, J. Alloy. Compd. 649 (2015) 585–590.
CoCrFeNiAl	BCC	Y.J. Zhou, Y. Zhang, Y.L. Wang, G.L. Chen, Appl. Phys. Lett. 90 (2007) 181904.
CoCrFeNiCu	FCC	<p>J.W. Yeh, S.K. Chen, S.J. Lin, J.Y. Gan, T.S. Chin, T.T. Shun, C.H. Tsau, S.Y. Chang, Adv. Eng. Mater. 6 (2004) 299–303.</p>
CoCrFeNiCuAl0.3	FCC	
CoCrFeNiCuAl0.5	FCC	
CoCrFeNiCuAl0.8	FCC+BCC	
CoCrFeNiCuAl	FCC+BCC	
CoCrFeNiCuAl1.3	FCC+BCC	
CoCrFeNiCuAl1.5	FCC+BCC	
CoCrFeNiCuAl1.8	FCC+BCC	
CoCrFeNiCuAl2	FCC+BCC	
CoCrFeNiCuAl2.3	BCC	
CoCrFeNiCuAl2.5	BCC	
CoCrFeNiCuAl2.8	BCC	
CoCrFeNiCuAl3	BCC	
CoCrFeNiCuAlSi	FCC+BCC	<p>J.W. Yeh, S.Y. Chang, Y.D. Hong, S.K. Chen, S.J. Lin, Mater. Chem. Phys. 103 (2007) 41–46.</p>
CoCrNiCuAl	FCC+BCC	
CoCuNiAl	FCC+BCC	
CuNiAl	FCC+BCC	
MnCrFeNiCuAl	BCC	H.Y. Chen, C.W. Tsai, C.C. Tung, J.W. Yeh, T.T. Shun, C.C. Yang, S.K. Chen, Ann. Chim. Sci. Mater. 31 (2006) 685–698.
FeCoNiCrMn	FCC	<p>B. Cantor, I.T.H. Chang, P. Knight, A.J.B. Vincent, Mater. Sci. Eng., A 375–377 (2004) 213–218.</p>
CoCrFeNiMnCu	FCC	

CoCrNiCu0.5Al	BCC	J.W. Yeh, S.J. Lin, T.S. Chin, J.Y. Gan, S.K. Chen, T.T. Shun, C.H. Tsau, S.Y. Chou, Metall. Mater. Trans. A 35 (2004) 2533–2536.
TiCoCrFeNiCuAlV	FCC+BCC	
Co0.5CrFeNiCuAl	FCC+BCC	
CoCr0.5FeNiCuAl	FCC+BCC	
CoCrFe0.5NiCuAl	FCC+BCC	
CoCrFeNi0.5CuAl	FCC+BCC	
CoCrFeNiCu0.5Al	BCC	
Cu0.5NiCoCrAl0.5Fe2	FCC	Ke, G.-Y., Chen, G.-Y., Hsu, T. & Yeh, J.-W. FCC and BCC equivalents in as-cast solid solutions of Al _x CoyCrzCu0.5FevNi _w high-entropy alloys. Ann. Chim. 31, 669–683 (2006).
TiCr0.5FeNiCuAl	FCC+BCC	
TiCrFeNiCuAl	FCC+BCC	
TiCr1.5FeNiCuAl	FCC+BCC	M. Chen, Y. Liu, Y.X. Li, X. Chen, Acta Metall. Sin. 43 (2007) 1020–1024
TiCr2FeNiCuAl	FCC+BCC	
TiCr3FeNiCuAl	FCC+BCC	
CoCrFeNiCuAlV	FCC+BCC	B.S. Li, Y.R. Wang, M.X. Ren, C. Yang, H.Z. Fu, Mater. Sci. Eng. A 498 (2008) 482–486.
Ti0.5Co1.5CrFeNiAl	FCC+BCC	
Ti0.5Co2CrFeNiAl	FCC+BCC	
Ti0.5Co3CrFeNiAl	FCC+BCC	F.J. Wang, Y. Zhang, Mater. Sci. Eng. A 496 (2008) 214–216.
Ti0.5CoCrFeNiCu0.75Al0.25	FCC	
Ti0.5CoCeFeNiCu0.5Al0.5	FCC+BCC	F.J. Wang, Y. Zhang, G.L. Chen, J. Alloys Compd. 478 (2009) 321–324.
CoCrFeNiCu0.25Al	BCC	
CoFeNiCuV	FCC	Y. Zhang, Y.J. Zhou, J.P. Lin, G.L. Chen, P.K. Liaw, Adv. Eng. Mater. 10 (2008) 534–538.
CoCrFeNiCu0.75Al0.25	FCC	
CoCrFeNiCu0.5Al0.5	FCC	
CoCrFeNiCu0.25Al0.75	FCC+BCC	Y.J. Zhou, Y. Zhang, F.J. Wang, G.L. Chen, Appl. Phys. Lett. 92 (2008) 241917
CoCrFeNiAl0.25	FCC	
CoCrFeNiAl0.375	FCC	
CoCrFeNiAl0.5	FCC+BCC	
CoCrFeNiAl0.75	FCC+BCC	H.P. Chou, Y.S. Chang, S.K. Chen, J.W. Yeh, Mater. Sci. Eng., B 163 (2009) 184–189
CoCrFeNiAl0.875	FCC+BCC	
CoCrFeNiAl1.25	BCC	
CoCrFeNiAl1.5	BCC	
CoCrFeNiAl2	BCC	
CoCrFeNiAl2.5	BCC	
CoCrFeNiAl3	BCC	C. Li, J.C. Li, M. Zhao, Q. Jiang, J. Alloys Compd. 475 (2009) 752–757.
MoCrFeNiCu	FCC	

MnCrFeNiCu	FCC+BCC	
MnCrFe1.5Ni0.5Al0.3	BCC	K.C. Hsieh, C.F. Yu, W.T. Hsieh, W.R. Chiang, J.S. Ku, J.H. Lai, C.P. Tu, C.C. Yang, <i>J. Alloys Compd.</i> 483 (2009) 209–212.
MnCrFe1.5Ni0.5Al0.5	BCC	
Ti0.5Co1.5CrFeNi1.5	FCC	Y.L. Chou, J.W. Yeh, H.C. Shih, <i>Corros. Sci.</i> 52 (2010) 2571–2581.
Ti0.5Co1.5CrFeNi1.5Mo0.1	FCC	
CoCrFeNiCuAl0.5V0.2	FCC	
CoCrFeNiCuAl0.5V0.4	FCC+BCC	
CoCrFeNiCuAl0.5V1.2	FCC+BCC	M.R. Chen, S.J. Lin, J.W. Yeh, M.H. Chuang, S.K. Chen, Y.S. Huang, <i>Metall. Mater. Trans. A</i> 37 (2006) 1363–1369.
CoCrFeNiCuAl0.5V1.4	FCC+BCC	
CoCrFeNiCuAl0.5V1.6	FCC+BCC	
CoCrFeNiCuAl0.5V1.8	FCC+BCC	
CoCrFeNiCuAl0.5V2	FCC+BCC	
Mn2CrFeNi2Cu	FCC	
MnCr2Fe2NiCu	FCC+BCC	
Mn2Cr2Fe2Ni2Cu	FCC	
Mn2CrFe2NiCu2	FCC+BCC	B. Ren, Z.X. Liu, D.M. Li, L. Shi, B. Cai, M.X. Wang, <i>J. Alloys Compd.</i> 493 (2010) 148–153.
MnCrFe2Ni2Cu2	FCC	
Mn2Cr2FeNi2Cu2	FCC+BCC	
MnCr2Fe2Ni2Cu2	FCC+BCC	
W27.3Nb22.7Mo25.6Ta24.4	BCC	O.N. Senkov, G.B. Wilks, D.B. Miracle, C.P. Chuang, P.K. Liaw, <i>Intermetallics</i> 18 (2010) 1758–1765.
W21.1Nb20.6Mo21.7Ta15.6V21	BCC	
CoCrFeNiMo0.3	FCC	T.T. Shun, C.H. Hung, C.F. Lee, <i>J. Alloys Compd.</i> 493 (2010) 105–109
CoCrFeNiAl0.3Mo0.1	FCC	
CoCrFeNiCuAlMo0.2	FCC+BCC	J.M. Zhu, H.F. Zhang, H.M. Fu, A.M. Wang, H. Li, Z.Q. Hu, <i>J. Alloys Compd.</i> 497 (2010) 52–56.
Al0.25CrCuFeNi2	FCC	
Al0.5CrCuFeNi2	FCC	
Al2.0CrCuFeNi2	BCC	Zhang Y, Lu ZP, Ma SG, Liaw PK, Tang Z, Cheng YQ, Gao MC (2014) Guidelines in predicting phase formation of high-entropy alloys. <i>MRS Commun</i> 4(2):57–62.
AlCoCrFeNiNb0.1	BCC	Ma SG, Zhang Y (2012) Effect of Nb addition on the microstructure and properties of AlCoCrFeNi high-entropy alloy. <i>Mater Sci Eng A</i> 532:480–486.
Al1.5CoCrFeNiTi	BCC	Zhang KB, Fu ZY (2012) Effects of annealing treatment on phase composition and microstructure of CoCrFeNiTiAlx high-entropy alloys. <i>Intermetallics</i> 22:24–32.
Al2CoCrFeNiTi	BCC	

Al0.2Co1.5CrFeNi1.5Ti0.5	FCC	Chuang MH, Tsai MH, Wang WR, Lin SJ, Yeh JW (2011) Microstructure and wear behavior of AlxCo1.5CrFeNi1.5Ti_y high-entropy alloys. Acta Mater 59(16):6308–6317.
CoCrFeNiPd	FCC	
CoCrFeNiPd2	FCC	Lucas MS, Mauger L, Munoz JA, Xiao YM, Sheets AO, Semiatin SL, Horwath J, Turgut Z (2011) Magnetic and vibrational properties of high-entropy alloys. J Appl Phys 109 (7):07E307.
AlCoCrFeNiSi0.6	BCC	
AlCoCrFeNiSi0.4	BCC	
AlCoCrFeNiSi0.2	BCC	Zhu JM, Fu HM, Zhang HF, Wang AM, Li H, Hu ZQ (2010) Synthesis and properties of multiprincipal component AlCoCrFeNiSix alloys. Mater Sci Eng A 527(27–28):7210–7214

Data S2. The data set used in the current work (separate file)

The data set used in our machine learning model contains 266 MPEAs consisting of 103 BCC, 61 FCC, and 102 BCC + FCC phases. Meanwhile, the values of 12 physical features of each MPEA are calculated.

Alloys	Phase	Diff_S	Diff_H	Tm	Ome ga	Diff_X	Diff_D	VE C	Gam ma	Densit y	Young 's Modul us	Bulk Modul us	Lamda
Al0.10CoCrFeMnNi	FCC	13.921	-5.244	1784.1 86	4.736	13.870	3.695	7.90 2	1.169	7.959	216.47 1	160.31 4	1.020
Al0.20CoCrFeMnNi	FCC	14.222	-6.243	1767.8 26	4.027	13.895	4.044	7.80 8	1.169	7.857	213.65 4	158.69 2	0.870
Al0.25CoCrCu0.5FeNiTi 0.5	FCC	15.433	-9.088	1784.7 08	3.031	12.828	5.587	7.85 7	1.196	7.677	198.00 0	158.85 7	0.494
Al0.25CoCrCu0.75FeNiTi 0.5	FCC	15.547	-7.281	1765.2 99	3.769	12.737	5.459	8.00 0	1.196	7.735	194.90 9	158.00 0	0.522
Al0.25CoCrFeNi	FCC	12.708	-6.754	1816.5 57	3.418	10.603	3.478	7.94 1	1.170	7.897	215.64 7	166.82 4	1.051
Al0.25CoFeNi	FCC	10.686	-6.059	1704.7 28	3.006	7.700	3.945	8.53 8	1.169	8.115	196.15 4	168.92 3	0.687
Al0.25MoNbTiV	BCC	12.708	-6.256	2353.7 34	4.781	24.322	4.003	4.88 2	1.120	7.077	163.64 7	162.11 8	0.793
Al0.25NbTaTiV	BCC	12.708	-4.817	2446.4 39	6.454	5.018	3.832	4.64 7	1.119	8.606	130.00 0	155.05 9	0.865
Al0.2Co1.5CrFeNi1.5Ti0. 5	FCC	13.671	-12.404	1823.1 92	2.009	12.514	5.342	7.91 2	1.195	7.825	206.22 8	164.94 7	0.479
Al0.375CoCrFeNi	FCC	12.970	-7.993	1791.3 26	2.906	10.957	4.117	7.80 0	1.170	7.748	211.48 6	164.22 9	0.765
Al0.38CoCrFeMnNi	FCC	14.558	-7.847	1739.9 11	3.228	13.925	4.542	7.64 7	1.169	7.684	208.84 8	155.92 6	0.706
Al0.3CoCrCuFe	FCC	12.825	2.747	1720.1 72	8.030	10.531	3.718	8.11 6	1.169	7.846	197.67 4	156.46 5	0.928
Al0.3CrFe1.5MnNi0.5	FCC+ BCC	12.319	-5.506	1758.0 33	3.934	12.969	4.703	7.18 6	1.168	7.373	212.67 4	150.65 1	0.557

Al0.3HfNbTaTiZr	BCC	14.432	-5.269	2433.0 27	6.664	12.038	4.977	4.32 1	1.133	9.511	108.30 2	129.01 9	0.583
Al0.3NbTa0.8Ti1.4V0.2Z r1.3	BCC	13.463	-7.485	2316.4 88	4.167	10.660	5.305	4.34 0	1.237	7.750	110.24 0	126.22 0	0.478
Al0.3NbTaTi1.4Zr1.3	BCC	12.631	-7.030	2360.7 68	4.241	10.318	4.845	4.34 0	1.133	8.174	112.56 0	127.82 0	0.538
Al0.43CoCrFeMnNi	FCC+ BCC	14.622	-8.252	1732.4 85	3.070	13.929	4.658	7.60 4	1.169	7.638	207.56 9	155.19 0	0.674
Al0.49CoCrFeMnNi	FCC+ BCC	14.687	-8.718	1723.7 52	2.904	13.933	4.787	7.55 4	1.169	7.584	206.06 6	154.32 4	0.641
Al0.4CrCuFeNi2	FCC	12.451	-1.701	1699.6 46	12.44 1	11.040	3.859	8.55 6	1.169	7.947	194.07 4	159.33 3	0.836
Al0.4Hf0.6NbTaTiZr	BCC	14.500	-7.770	2397.1 98	4.474	11.584	4.923	4.32 0	1.133	9.071	109.96 0	129.48 0	0.598
Al0.56CoCrFeMnNi	FCC+ BCC	14.749	-9.233	1713.8 03	2.738	13.936	4.925	7.49 6	1.169	7.523	204.35 3	153.33 8	0.608
Al0.5CoCrCu0.5FeNiTi0. 5	FCC+ BCC	15.745	-10.843	1746.0 15	2.535	13.088	5.968	7.63 6	1.196	7.450	192.18 2	155.09 1	0.442
Al0.5CoCrCuFe	FCC	13.145	0.889	1685.2 08	24.92 1	11.036	4.491	7.88 9	1.169	7.617	192.00 0	152.88 9	0.652
Al0.5CoCrCuFeNi	FCC	14.697	-1.521	1692.9 88	16.36 3	10.933	4.169	8.27 3	1.170	7.852	193.45 5	157.81 8	0.846
Al0.5CoCrCuFeNiTi	FCC+ BCC	16.005	-11.598	1731.1 44	2.389	14.139	6.535	7.61 5	1.196	7.341	181.53 8	150.46 2	0.375
Al0.5CoCrCuFeNiTi0.2	FCC	15.445	-4.149	1701.6 90	6.335	11.875	4.931	8.12 3	1.196	7.735	190.73 7	156.14 0	0.635
Al0.5CoCrCuFeNiTi0.4	FCC	15.762	-6.423	1709.8 03	4.196	12.624	5.491	7.98 3	1.196	7.627	188.20 3	154.57 6	0.523
Al0.5CoCrCuFeNiTi0.6	FCC+ BCC	15.924	-8.396	1717.3 83	3.257	13.231	5.922	7.85 2	1.196	7.525	185.83 6	153.11 5	0.454
Al0.5CoCrCuFeNiTi0.8	FCC+ BCC	15.995	-10.108	1724.4 82	2.729	13.728	6.262	7.73 0	1.196	7.430	183.61 9	151.74 6	0.408
Al0.5CoCrCuFeNiTi1.2	FCC+ BCC	15.973	-12.894	1737.4 08	2.152	14.480	6.756	7.50 7	1.196	7.257	179.58 2	149.25 4	0.350
Al0.5CoCrCuFeNiTi1.4	FCC+ BCC	15.909	-14.022	1743.3 09	1.978	14.764	6.938	7.40 6	1.196	7.178	177.73 9	148.11 6	0.331
Al0.5CoCrCuFeNiTi1.6	FCC+	15.821	-15.005	1748.8	1.844	15.001	7.086	7.31	1.196	7.103	176.00	147.04	0.315

	BCC			78				0			0	2	
Al0.5CoCrCuFeNiTi1.8	FCC+ BCC	15.717	-15.860	1754.1 42	1.738	15.199	7.209	7.21 9	1.196	7.033	174.35 6	146.02 7	0.302
Al0.5CoCrCuFeNiTi2	FCC+ BCC	15.599	-16.604	1759.1 25	1.653	15.363	7.309	7.13 3	1.196	6.966	172.80 0	145.06 7	0.292
Al0.5CoCrCuFeNiV0.2	FCC	15.445	-2.499	1710.1 82	10.56 9	11.268	4.146	8.15 8	1.169	7.790	191.15 8	157.89 5	0.899
Al0.5CoCrCuFeNiV0.4	FCC+ BCC	15.762	-3.344	1726.2 09	8.137	11.539	4.120	8.05 1	1.169	7.733	189.01 7	157.96 6	0.929
Al0.5CoCrCuFeNiV0.6	FCC+ BCC	15.924	-4.074	1741.1 86	6.806	11.759	4.093	7.95 1	1.169	7.680	187.01 6	158.03 3	0.951
Al0.5CoCrCuFeNiV0.8	FCC+ BCC	15.995	-4.706	1755.2 12	5.965	11.936	4.065	7.85 7	1.169	7.630	185.14 3	158.09 5	0.968
Al0.5CoCrCuFeNiV1.0	FCC+ BCC	16.005	-5.254	1768.3 75	5.387	12.079	4.036	7.76 9	1.169	7.583	183.38 5	158.15 4	0.983
Al0.5CoCrCuFeNiV1.2	BCC	15.973	-5.730	1780.7 51	4.964	12.193	4.006	7.68 7	1.169	7.539	181.73 1	158.20 9	0.995
Al0.5CoCrCuFeNiV1.4	BCC	15.909	-6.142	1792.4 11	4.643	12.284	3.976	7.60 9	1.169	7.497	180.17 4	158.26 1	1.006
Al0.5CoCrCuFeNiV1.6	BCC	15.821	-6.499	1803.4 13	4.391	12.354	3.946	7.53 5	1.169	7.458	178.70 4	158.31 0	1.016
Al0.5CoCrCuFeNiV1.8	BCC	15.717	-6.808	1813.8 13	4.187	12.407	3.916	7.46 6	1.169	7.421	177.31 5	158.35 6	1.025
Al0.5CoCrCuFeNiV2.0	BCC	15.599	-7.076	1823.6 58	4.021	12.446	3.886	7.40 0	1.169	7.385	176.00 0	158.40 0	1.033
Al0.5CoCrFeNi	FCC+ BCC	13.145	-9.086	1767.4 97	2.557	11.255	4.602	7.66 7	1.170	7.608	207.55 6	161.77 8	0.621
Al0.5CoFeNi	FCC+ BCC	11.239	-9.469	1649.6 39	1.958	9.708	5.123	8.14 3	1.169	7.727	187.14 3	162.28 6	0.428
Al0.5CrCuFeNi2	FCC	12.602	-2.512	1685.7 15	8.455	11.309	4.200	8.45 5	1.169	7.852	191.81 8	157.81 8	0.715
Al0.5CrFe1.5MnNi0.5	BCC	12.662	-7.259	1721.3 86	3.002	12.876	5.163	7.00 0	1.168	7.164	206.33 3	147.33 3	0.475
Al0.5HfNbTaTiZr	BCC	14.697	-8.860	2378.4 97	3.946	12.134	4.960	4.27 3	1.133	9.263	106.90 9	127.09 1	0.598
Al0.5MoNbTiV	BCC	13.145	-8.988	2274.8 30	3.327	23.783	3.932	4.77 8	1.120	6.833	158.44 4	157.33 3	0.850

Al0.5NbTa0.8Ti1.5V0.2Zr	BCC	13.778	-10.778	2264.9₆₇	2.895	9.972	4.927	4.30₀	1.237	7.558	111.28₀	127.20₀	0.568
Al0.5NbTaTiV	BCC	13.145	-8.395	2362.3₈₆	3.699	4.962	3.738	4.55₆	1.119	8.277	126.66₇	150.66₇	0.941
Al0.62CoCrFeMnNi	FCC+ BCC	14.791	-9.653	1705.4₇₂	2.613	13.936	5.033	7.44₈	1.169	7.471	202.91₈	152.51₂	0.584
Al0.68CoCrFeMnNi	FCC+ BCC	14.825	-10.053	1697.3₁₇	2.503	13.934	5.134	7.40₁	1.169	7.421	201.51₄	151.70₄	0.562
Al0.6CrCuFeNi2	FCC	12.720	-3.265	1672.2₈₃	6.514	11.551	4.489	8.35₇	1.169	7.760	189.64₃	156.35₇	0.631
Al0.75CoCrCu0.25FeNiTi0.5	FCC+ BCC	15.547	-14.388	1726.7₃₂	1.866	13.299	6.381	7.27₃	1.196	7.165	189.45₅	152.18₂	0.382
Al0.75CoCrFeMnNi	FCC+ BCC	14.855	-10.495	1688.0₁₈	2.389	13.931	5.243	7.34₈	1.169	7.363	199.91₃	150.78₃	0.540
Al0.75CoCrFeNi	FCC+ BCC	13.332	-10.903	1723.6₀₁	2.108	11.721	5.301	7.42₁	1.170	7.349	200.31₆	157.26₃	0.474
Al0.75CoFeNi	FCC+ BCC	11.467	-11.947	1601.8₉₄	1.538	10.939	5.805	7.80₀	1.169	7.391	179.33₃	156.53₃	0.340
Al0.75HfNbTaTiZr	BCC	14.855	-12.643	2315.6₇₀	2.721	12.215	4.933	4.21₇	1.133	8.977	105.30₄	124.87₀	0.610
Al0.75MoNbTiV	BCC	13.332	-11.125	2204.2₃₂	2.642	23.276	3.863	4.68₄	1.120	6.615	153.78₉	153.05₃	0.893
Al0.7Co0.3CrFeNi	FCC+ BCC	12.795	-11.397	1725.7₀₇	1.937	11.918	5.538	7.20₀	1.170	7.134	200.42₅	154.30₀	0.417
Al0.81CoCrFeMnNi	FCC+ BCC	14.873	-10.856	1680.2₂₆	2.302	13.927	5.329	7.30₃	1.169	7.315	198.57₁	150.01₀	0.524
Al0.875CoCrFeNi	FCC+ BCC	13.370	-11.655	1703.3₄₁	1.954	11.902	5.560	7.30₈	1.170	7.229	196.97₄	155.17₉	0.432
Al0.88CoCrFeMnNi	FCC+ BCC	14.888	-11.255	1671.3₃₆	2.211	13.920	5.422	7.25₂	1.169	7.260	197.04₁	149.12₉	0.506
Al0.8CoCrCuFe	FCC+ BCC	13.351	-1.354	1638.2₂₄	16.15₁	11.581	5.238	7.58₃	1.169	7.309	184.37₅	148.08₃	0.487
Al0.8CoCrCuFeNi	FCC+ BCC	14.871	-3.615	1653.7₀₃	6.803	11.578	4.922	8.00₀	1.170	7.585	187.06₉	153.58₆	0.614
Al0.8CrCuFeNi2	FCC	12.884	-4.614	1646.8₀₆	4.599	11.963	4.956	8.17₂	1.169	7.585	185.51₇	153.58₆	0.525
Al0.95CoCrFeMnNi	FCC+	14.895	-11.632	1662.6	2.129	13.911	5.508	7.20	1.169	7.206	195.54	148.26	0.491

	BCC			55				2			6	9	
Al1.125CuFe0.75NiTi1.1 25	FCC	13.299	-19.955	1535.5 46	1.023	15.777	7.168	6.97 5	1.194	6.378	139.50 0	131.35 0	0.259
Al1.25CoCrFeMnNi	BCC	14.865	-13.030	1627.6 54	1.857	13.860	5.810	7.00 0	1.169	6.989	189.52 0	144.80 0	0.440
Al1.25CoCrFeNi	BCC	13.345	-13.424	1648.3 50	1.639	12.298	6.118	7.00 0	1.170	6.905	187.90 5	149.52 4	0.357
Al1.2CrCuFeNi2	FCC+ BCC	13.017	-6.785	1600.7 85	3.071	12.570	5.603	7.83 9	1.169	7.269	178.06 5	148.58 1	0.415
Al1.3CoCrCuFe	FCC+ BCC	13.330	-4.030	1571.7 38	5.199	12.125	5.948	7.15 1	1.169	6.873	173.58 5	141.28 3	0.377
Al1.3CoCrCuFeNi	FCC+ BCC	14.852	-6.238	1596.5 41	3.801	12.294	5.686	7.60 3	1.170	7.196	177.77 8	147.42 9	0.459
Al1.5CoCrCuFe	FCC+ BCC	13.254	-4.826	1548.5 28	4.252	12.258	6.126	7.00 0	1.169	6.721	169.81 8	138.90 9	0.353
Al1.5CoCrCuFeNi	FCC+ BCC	14.784	-7.053	1576.1 39	3.304	12.493	5.893	7.46 2	1.170	7.058	174.46 2	145.23 1	0.426
Al1.5CoCrFeNi	BCC	13.254	-14.281	1615.8 55	1.500	12.469	6.365	6.81 8	1.170	6.714	182.54 5	146.18 2	0.327
Al1.5CoCrFeNiTi	BCC	14.784	-22.722	1665.8 78	1.084	14.005	7.292	6.38 5	1.195	6.378	172.30 8	140.61 5	0.278
Al1.8CoCrCuFe	FCC+ BCC	13.098	-5.803	1516.7 15	3.424	12.396	6.323	6.79 3	1.169	6.512	164.65 5	135.65 5	0.328
Al1.8CoCrCuFeNi	FCC+ BCC	14.644	-8.080	1547.7 86	2.805	12.726	6.133	7.26 5	1.170	6.865	169.85 3	142.17 6	0.389
Al2.0CoCrCuFe	FCC+ BCC	12.976	-6.333	1497.2 73	3.068	12.455	6.418	6.66 7	1.169	6.385	161.50 0	133.66 7	0.315
Al2.0CrCuFeNi2	BCC	12.885	-9.633	1524.5 20	2.039	13.243	6.297	7.28 6	1.169	6.746	165.71 4	140.28 6	0.325
Al2.3CoCrCuFe	FCC+ BCC	12.774	-6.984	1470.4 26	2.689	12.507	6.522	6.49 2	1.169	6.209	157.14 3	130.92 1	0.300
Al2.3CoCrCuFeNi	FCC+ BCC	14.345	-9.375	1505.7 10	2.304	12.980	6.403	6.97 3	1.170	6.579	163.01 4	137.64 4	0.350
Al2.5CoCrCuFe	FCC+ BCC	12.632	-7.337	1453.9 04	2.503	12.522	6.571	6.38 5	1.169	6.101	154.46 2	129.23 1	0.293
Al2.5CoCrCuFeNi	FCC+ BCC	14.213	-9.778	1490.4 50	2.166	13.046	6.478	6.86 7	1.170	6.475	160.53 3	136.00 0	0.339

Al2.5CoCrFeNi	BCC	12.632	-16.095	1510.8 73	1.186	12.725	6.842	6.23 1	1.170	6.095	165.23 1	135.38 5	0.270
Al2.8CoCrCuFe	BCC	12.412	-7.768	1430.9 44	2.286	12.520	6.619	6.23 5	1.169	5.950	150.73 5	126.88 2	0.283
Al2.8CoCrCuFeNi	BCC	14.005	-10.283	1469.0 28	2.001	13.117	6.566	6.71 8	1.170	6.330	157.05 1	133.69 2	0.325
Al2CoCrCuFeNi	FCC+ BCC	14.532	-8.653	1530.2 34	2.570	12.844	6.257	7.14 3	1.170	6.746	167.00 0	140.28 6	0.371
Al2CoCrFeMo0.5Ni	BCC	14.232	-14.296	1661.8 37	1.654	16.351	6.491	6.46 2	1.169	6.672	185.15 4	147.23 1	0.338
Al2CoCrFeNi	BCC	12.976	-15.444	1558.9 90	1.310	12.662	6.678	6.50 0	1.170	6.378	173.16 7	140.33 3	0.291
Al2CoCrFeNiTi	BCC	14.532	-23.347	1613.5 63	1.004	13.836	7.299	6.14 3	1.195	6.114	165.00 0	136.00 0	0.273
Al3.0CoCrCuFe	BCC	12.264	-8.000	1416.7 30	2.172	12.506	6.639	6.14 3	1.169	5.857	148.42 9	125.42 9	0.278
Al3CoCrCuFeNi	BCC	13.863	-10.563	1455.6 39	1.911	13.148	6.610	6.62 5	1.170	6.239	154.87 5	132.25 0	0.317
Al3CoCrFeNi	BCC	12.264	-16.408	1469.6 30	1.098	12.705	6.916	6.00 0	1.170	5.851	158.42 9	131.14 3	0.256
AlCo2CrFeMo0.5Ni	FCC+ BCC	14.232	-10.698	1790.2 26	2.382	14.824	5.437	7.38 5	1.169	7.629	206.53 8	163.23 1	0.482
AlCoCrCuFe	FCC+ BCC	13.381	-2.560	1610.0 34	8.415	11.842	5.580	7.40 0	1.169	7.124	179.80 0	145.20 0	0.430
AlCoCrCuFeMnNi	FCC+ BCC	16.178	-5.633	1613.8 81	4.635	14.038	5.183	7.71 4	1.169	7.423	185.28 6	146.57 1	0.602
AlCoCrCuFeNi	FCC+ BCC	14.897	-4.778	1629.6 95	5.081	11.908	5.281	7.83 3	1.170	7.422	183.16 7	151.00 0	0.534
AlCoCrCuFeNiTi	FCC+ BCC	16.178	-13.796	1674.1 67	1.963	14.257	6.778	7.28 6	1.196	7.009	173.57 1	145.14 3	0.352
AlCoCrCuFeNiV	FCC+ BCC	16.178	-7.755	1708.7 39	3.565	12.500	4.954	7.42 9	1.169	7.233	175.28 6	152.28 6	0.659
AlCoCrCuNiTi	BCC	14.897	-16.667	1651.3 62	1.476	15.100	6.900	7.16 7	1.190	6.863	167.33 3	141.00 0	0.313
AlCoCrFeMo0.1Ni	BCC	13.921	-12.134	1707.8 57	1.959	13.060	5.778	7.17 6	1.169	7.176	196.45 1	154.70 6	0.417
AlCoCrFeMo0.5Ni1.5	FCC+	14.534	-11.528	1788.7	2.255	15.457	5.610	7.33	1.169	7.523	205.58	161.83	0.462

	BCC			45				3			3	3	
AlCoCrFeMo0.5Ni2	FCC+ BCC	14.232	-11.456	1784.0 72	2.217	15.039	5.471	7.53 8	1.169	7.629	205.15 4	163.23 1	0.476
AlCoCrFeNb0.1Ni	BCC	13.921	-13.318	1704.9 94	1.782	12.190	5.919	7.15 7	1.168	7.145	192.05 9	153.52 9	0.397
AlCoCrFeNi	BCC	13.381	-12.320	1684.0 94	1.829	12.057	5.778	7.20 0	1.170	7.116	193.80 0	153.20 0	0.401
AlCoCrFeNiNb0.1	BCC	13.921	-13.318	1704.9 94	1.782	12.190	5.919	7.15 7	1.168	7.145	192.05 9	153.52 9	0.397
AlCoCrFeNiSi	BCC	14.897	-27.333	1684.5 78	0.918	11.908	6.611	6.66 7	1.265	6.317	169.33 3	144.33 3	0.341
AlCoCrFeNiSi0.2	BCC	14.222	-16.391	1684.2 06	1.461	12.053	6.018	7.07 7	1.265	6.932	188.15 4	151.15 4	0.393
AlCoCrFeNiSi0.4	BCC	14.585	-19.835	1684.3 09	1.238	12.033	6.214	6.96 3	1.265	6.761	182.92 6	149.25 9	0.378
AlCoCrFeNiSi0.6	BCC	14.778	-22.755	1684.4 05	1.094	12.001	6.373	6.85 7	1.265	6.602	178.07 1	147.50 0	0.364
AlCoCrFeNiTi	BCC	14.897	-21.556	1726.9 12	1.193	14.135	7.221	6.66 7	1.195	6.685	180.83 3	146.00 0	0.286
AlCoCrFeNiTi0.5	BCC	14.697	-17.917	1707.4 49	1.401	13.378	6.718	6.90 9	1.195	6.881	186.72 7	149.27 3	0.326
AlCoCuFeNi	FCC+ BCC	13.381	-5.280	1519.6 34	3.851	11.146	5.609	8.20 0	1.169	7.468	164.00 0	149.20 0	0.425
AlCoCuFeNiSi	FCC+ BCC	13.381	-19.840	1511.4 34	1.019	11.002	7.141	7.00 0	1.264	6.150	133.40 0	133.20 0	0.262
AlCoCuFeNiTi	FCC+ BCC	13.381	-15.520	1562.2 34	1.347	14.797	7.091	7.00 0	1.194	6.592	147.20 0	135.20 0	0.266
AlCoCuFeNiZr	FCC+ BCC	13.381	-23.360	1599.6 34	0.916	21.624	10.234	7.00 0	1.323	6.986	137.60 0	127.40 0	0.128
AlCoFeNi	BCC	11.526	-13.750	1560.1 18	1.308	11.755	6.237	7.50 0	1.169	7.098	172.50 0	151.50 0	0.296
AlCoFeNiTiVZr	BCC	16.178	-32.163	1784.6 39	0.898	19.449	9.413	6.14 3	1.322	6.503	143.14 3	135.28 6	0.183
AlCr0.5NbTiV	BCC	13.145	-15.407	1977.2 16	1.687	3.765	5.233	4.44 4	1.183	5.664	124.11 1	132.44 4	0.480
AlCrCuFeNi	FCC+ BCC	13.381	-4.000	1602.0 34	5.359	12.416	5.628	7.60 0	1.169	7.124	178.00 0	145.20 0	0.422

AlCrCuFeNi0.6	FCC+ BCC	13.242	-2.684	1591.0 80	7.849	12.332	5.760	7.39 1	1.169	6.969	176.08 7	142.17 4	0.399
AlCrCuFeNi0.8	FCC+ BCC	13.351	-3.403	1596.7 85	6.265	12.388	5.694	7.50 0	1.169	7.050	177.08 3	143.75 0	0.412
AlCrCuFeNi1.2	FCC+ BCC	13.357	-4.497	1606.8 79	4.773	12.421	5.563	7.69 2	1.169	7.193	178.84 6	146.53 8	0.432
AlCrCuFeNi1.4	FCC+ BCC	13.295	-4.911	1611.3 65	4.363	12.409	5.500	7.77 8	1.169	7.256	179.63 0	147.77 8	0.440
AlCrCuFeNi2	FCC+ BCC	12.976	-5.778	1623.0 28	3.645	12.297	5.317	8.00 0	1.169	7.422	181.66 7	151.00 0	0.459
AlCrFeNi	BCC	11.526	-13.250	1663.1 18	1.447	12.214	6.260	6.75 0	1.169	6.668	190.00 0	146.50 0	0.294
AlCrFeNiMo0.2	BCC	12.568	-12.653	1721.8 26	1.710	14.744	6.204	6.71 4	1.168	6.836	196.61 9	150.47 6	0.327
AlCrFeNiMo0.5	BCC	13.145	-11.852	1800.1 04	1.997	17.223	6.112	6.66 7	1.168	7.060	205.44 4	155.77 8	0.352
AlCuFeNiTi	FCC	13.381	-17.600	1554.2 34	1.182	15.354	7.162	7.20 0	1.194	6.592	145.40 0	135.20 0	0.261
AlCuNiTi	FCC	11.526	-23.250	1490.0 43	0.739	16.688	6.924	7.00 0	1.188	6.270	129.00 0	126.50 0	0.240
AlMo0.5NbTa0.5TiZr	BCC	14.533	-18.280	2169.0 94	1.725	21.761	5.041	4.30 0	1.192	7.148	123.30 0	128.40 0	0.572
AlMoNbTiV	BCC	13.381	-12.800	2140.6 94	2.238	22.798	3.796	4.60 0	1.120	6.419	149.60 0	149.20 0	0.928
AlNb1.5Ta0.5Ti1.5Zr0.5	BCC	12.511	-16.200	2135.7 94	1.649	8.112	3.481	4.20 0	1.133	6.788	105.70 0	126.30 0	1.033
AlNbTaTiV	BCC	13.381	-13.440	2219.4 94	2.210	4.841	3.567	4.40 0	1.119	7.719	121.00 0	143.20 0	1.052
AlNbTiV	BCC	11.526	-16.250	1951.8 68	1.384	3.354	3.947	4.25 0	1.119	5.473	104.75 0	129.00 0	0.740
Co0.5CrFeNiCuAl	FCC+ BCC	14.697	-5.686	1617.1 22	4.180	12.169	5.448	7.72 7	1.170	7.286	180.81 8	148.36 4	0.495
Co1.5CrFeNi1.5Ti0.5	FCC	12.858	-10.744	1855.5 45	2.221	12.187	4.885	8.09 1	1.197	8.012	211.18 2	168.18 2	0.539
CoCr0.5FeNiCuAl	FCC+ BCC	14.697	-6.479	1579.6 67	3.583	11.650	5.440	8.00 0	1.170	7.443	174.45 5	150.18 2	0.497
CoCrCuFeNiTi	FCC	14.897	-8.444	1797.6	3.171	13.876	6.117	8.00	1.197	7.728	190.83	156.66	0.398

				17				0			3	7	
CoCrCuFeNiTi0.5	FCC	14.697	-3.702	1784.5 82	7.084	12.236	4.822	8.36 4	1.197	8.019	197.63 6	160.90 9	0.632
CoCrFe0.5NiCuAl	FCC+ BCC	14.697	-3.504	1613.2 13	6.766	12.398	5.404	7.81 8	1.170	7.380	180.63 6	149.27 3	0.503
CoCrFeMnNi	FCC	13.381	-4.160	1801.2 00	5.794	13.836	3.269	8.00 0	1.096	8.064	219.40 0	162.00 0	1.252
CoCrFeMnNiV0.25	FCC	14.335	-5.297	1819.3 81	4.924	13.810	3.288	7.85 7	1.096	7.971	215.04 8	161.90 5	1.326
CoCrFeMnNiV0.5	FCC	14.697	-6.215	1835.9 09	4.342	13.759	3.295	7.72 7	1.096	7.886	211.09 1	161.81 8	1.354
CoCrFeNi0.5CuAl	FCC+ BCC	14.697	-4.562	1620.7 58	5.222	11.930	5.427	7.63 6	1.170	7.286	181.63 6	148.36 4	0.499
CoCrFeNiAl	BCC	13.381	-12.320	1684.0 94	1.829	12.057	5.778	7.20 0	1.170	7.116	193.80 0	153.20 0	0.401
CoCrFeNiAl0.25	FCC	12.708	-8.249	1816.5 57	2.798	10.603	3.478	7.94 1	1.170	7.897	215.64 7	166.82 4	1.051
CoCrFeNiAl0.375	FCC	12.970	-9.169	1791.3 26	2.534	10.957	4.117	7.80 0	1.170	7.748	211.48 6	164.22 9	0.765
CoCrFeNiAl0.3Mo0.1	FCC	13.436	-9.258	1831.0 55	2.657	11.870	3.903	7.84 1	1.169	7.890	216.56 8	167.22 7	0.882
CoCrFeNiAl0.5	FCC+ BCC	13.145	-9.975	1767.4 97	2.329	11.255	4.602	7.66 7	1.170	7.608	207.55 6	161.77 8	0.621
CoCrFeNiAl0.75	FCC+ BCC	13.332	-11.302	1723.6 01	2.033	11.721	5.301	7.42 1	1.170	7.349	200.31 6	157.26 3	0.474
CoCrFeNiAl0.875	FCC+ BCC	13.370	-11.845	1703.3 41	1.923	11.902	5.560	7.30 8	1.170	7.229	196.97 4	155.17 9	0.432
CoCrFeNiAl1.25	BCC	13.345	-13.098	1648.3 50	1.679	12.298	6.118	7.00 0	1.170	6.905	187.90 5	149.52 4	0.357
CoCrFeNiAl1.5	BCC	13.254	-13.686	1615.8 55	1.565	12.469	6.365	6.81 8	1.170	6.714	182.54 5	146.18 2	0.327
CoCrFeNiAl2	BCC	12.976	-14.444	1558.9 90	1.400	12.662	6.678	6.50 0	1.170	6.378	173.16 7	140.33 3	0.291
CoCrFeNiAl2.5	BCC	12.632	-14.817	1510.8 73	1.288	12.725	6.842	6.23 1	1.170	6.095	165.23 1	135.38 5	0.270
CoCrFeNiAl3	BCC	12.264	-14.939	1469.6 30	1.206	12.705	6.916	6.00 0	1.170	5.851	158.42 9	131.14 3	0.256

CoCrFeNiCu0.25Al	BCC	14.335	-3.302	1668.5 51	7.245	12.049	5.641	7.38 1	1.170	7.203	190.76 2	152.57 1	0.451
CoCrFeNiCu0.25Al0.75	FCC+ BCC	14.316	-2.830	1705.3 06	8.627	11.687	5.166	7.60 0	1.170	7.429	196.80 0	156.40 0	0.536
CoCrFeNiCu0.5Al	BCC	14.697	-3.901	1654.4 22	6.233	12.019	5.513	7.54 5	1.170	7.283	188.00 0	152.00 0	0.484
CoCrFeNiCu0.5Al0.5	FCC	14.533	-3.080	1726.5 17	8.147	11.118	4.370	8.00 0	1.170	7.742	199.80 0	159.60 0	0.761
CoCrFeNiCu0.75Al0.25	FCC	14.316	-3.310	1747.7 29	7.559	10.316	3.250	8.40 0	1.170	8.055	202.80 0	162.80 0	1.355
CoCrFeNiCuAl	FCC+ BCC	14.897	-4.778	1629.6 95	5.081	11.908	5.281	7.83 3	1.170	7.422	183.16 7	151.00 0	0.534
CoCrFeNiCuAl0.3	FCC	14.432	-4.030	1721.6 49	6.166	10.368	3.423	8.47 2	1.170	8.047	198.11 3	160.90 6	1.232
CoCrFeNiCuAl0.5	FCC	14.697	-4.298	1692.9 88	5.790	10.933	4.169	8.27 3	1.170	7.852	193.45 5	157.81 8	0.846
CoCrFeNiCuAl0.5V0.2	FCC	15.445	-5.737	1710.1 82	4.604	11.268	4.146	8.15 8	1.169	7.790	191.15 8	157.89 5	0.899
CoCrFeNiCuAl0.5V0.4	FCC+ BCC	15.762	-5.883	1726.2 09	4.625	11.539	4.120	8.05 1	1.169	7.733	189.01 7	157.96 6	0.929
CoCrFeNiCuAl0.5V1.2	FCC+ BCC	15.973	-6.202	1780.7 51	4.586	12.193	4.006	7.68 7	1.169	7.539	181.73 1	158.20 9	0.995
CoCrFeNiCuAl0.5V1.4	FCC+ BCC	15.909	-6.234	1792.4 11	4.574	12.284	3.976	7.60 9	1.169	7.497	180.17 4	158.26 1	1.006
CoCrFeNiCuAl0.5V1.6	FCC+ BCC	15.821	-6.253	1803.4 13	4.563	12.354	3.946	7.53 5	1.169	7.458	178.70 4	158.31 0	1.016
CoCrFeNiCuAl0.5V1.8	FCC+ BCC	15.717	-6.260	1813.8 13	4.554	12.407	3.916	7.46 6	1.169	7.421	177.31 5	158.35 6	1.025
CoCrFeNiCuAl0.5V2	FCC+ BCC	15.599	-6.258	1823.6 58	4.546	12.446	3.886	7.40 0	1.169	7.385	176.00 0	158.40 0	1.033
CoCrFeNiCuAl0.8	FCC+ BCC	14.871	-4.614	1653.7 03	5.330	11.578	4.922	8.00 0	1.170	7.585	187.06 9	153.58 6	0.614
CoCrFeNiCuAl1.3	FCC+ BCC	14.852	-4.969	1596.5 41	4.772	12.294	5.686	7.60 3	1.170	7.196	177.77 8	147.42 9	0.459
CoCrFeNiCuAl1.5	FCC+ BCC	14.784	-5.065	1576.1 39	4.601	12.493	5.893	7.46 2	1.170	7.058	174.46 2	145.23 1	0.426
CoCrFeNiCuAl1.8	FCC+	14.644	-5.173	1547.7	4.381	12.726	6.133	7.26	1.170	6.865	169.85	142.17	0.389

	BCC			86				5			3	6	
CoCrFeNiCuAl2	FCC+ BCC	14.532	-5.224	1530.2 34	4.256	12.844	6.257	7.14 3	1.170	6.746	167.00 0	140.28 6	0.371
CoCrFeNiCuAl2.3	BCC	14.345	-5.277	1505.7 10	4.093	12.980	6.403	6.97 3	1.170	6.579	163.01 4	137.64 4	0.350
CoCrFeNiCuAl2.5	BCC	14.213	-5.298	1490.4 50	3.998	13.046	6.478	6.86 7	1.170	6.475	160.53 3	136.00 0	0.339
CoCrFeNiCuAl2.8	BCC	14.005	-5.312	1469.0 28	3.873	13.117	6.566	6.71 8	1.170	6.330	157.05 1	133.69 2	0.325
CoCrFeNiCuAl3	BCC	13.863	-5.313	1455.6 39	3.799	13.148	6.610	6.62 5	1.170	6.239	154.87 5	132.25 0	0.317
CoCrFeNiCuAlSi	FCC+ BCC	16.178	-18.857	1637.8 81	1.405	11.585	6.126	7.28 6	1.265	6.693	163.71 4	143.71 4	0.431
CoCrFeNiCuAlV	FCC+ BCC	16.178	-7.755	1708.7 39	3.565	12.500	4.954	7.42 9	1.169	7.233	175.28 6	152.28 6	0.659
CoCrFeNiMnCu	FCC	14.897	1.444	1727.2 83	17.81 4	13.582	2.997	8.50 0	1.096	8.212	204.50 0	158.33 3	1.659
CoCrFeNiMo0.3	FCC	12.825	-4.154	1943.2 09	6.000	12.728	2.378	8.09 3	1.107	8.360	232.02 3	176.51 2	2.269
CoCrFeNiPd	FCC	13.381	-5.600	1863.0 00	4.452	17.488	4.040	8.60 0	1.118	8.978	204.00 0	174.00 0	0.820
CoCrFeNiPd2	FCC	12.976	-6.111	1857.1 67	3.943	19.576	4.695	8.83 3	1.118	9.482	190.16 7	175.00 0	0.589
CoCrFeNiTi	FCC	13.381	-16.320	1885.6 00	1.546	14.151	6.681	7.40 0	1.197	7.484	203.00 0	160.00 0	0.300
CoCrMnNi	FCC	11.526	-5.500	1798.7 50	3.769	15.050	3.447	8.00 0	1.091	8.110	221.50 0	160.00 0	0.970
CoCrNiCu0.5Al	BCC	13.145	-8.000	1619.6 27	2.661	13.115	5.805	7.44 4	1.164	7.150	182.88 9	148.00 0	0.390
CoCrNiCuAl	FCC+ BCC	13.381	-6.560	1593.4 34	3.250	12.952	5.524	7.80 0	1.164	7.330	177.60 0	147.20 0	0.438
CoCuFeMnNi	FCC	13.381	1.760	1636.7 40	12.44 4	13.485	3.179	9.00 0	1.096	8.416	189.60 0	158.00 0	1.324
CoCuFeMnNiSn0.03	FCC	13.604	1.772	1629.9 91	12.51 2	13.491	3.794	8.97 0	1.343	8.400	188.76 7	157.40 4	0.945
CoCuFeNiSn0.02	FCC	11.729	5.020	1660.3 98	3.880	3.126	2.344	9.47 3	1.343	8.648	186.81 6	166.95 5	2.134

CoCuNiAl	FCC+ BCC	11.526	-8.000	1446.7 93	2.084	12.460	5.852	8.25 0	1.164	7.365	152.25 0	144.00 0	0.337
CoFeMnNi	FCC	11.526	-4.000	1706.5 00	4.917	14.289	3.551	8.50 0	1.096	8.282	204.50 0	162.50 0	0.914
CoFeNiCuV	FCC	13.381	-2.240	1769.5 40	10.57 1	10.373	2.203	8.60 0	1.066	8.151	175.60 0	166.00 0	2.756
CoFeNiSi0.25	FCC	10.686	-11.834	1762.6 92	1.592	3.249	2.025	8.61 5	1.091	8.086	194.38 5	170.76 9	2.605
CoFeNiV	FCC	11.526	-10.500	1872.5 00	2.055	10.917	2.415	8.00 0	1.066	7.951	187.00 0	172.50 0	1.976
CoMnNi	FCC	9.134	-5.778	1671.6 67	2.643	16.310	3.735	8.66 7	1.091	8.417	202.33 3	160.00 0	0.655
CrCuFeMnNi	FCC+ BCC	13.381	2.720	1719.1 40	8.457	14.184	3.198	8.40 0	1.096	8.072	203.60 0	154.00 0	1.309
CrCuFeMoNi	FCC	13.381	4.640	1994.5 40	5.752	16.117	3.580	8.20 0	1.107	8.626	229.80 0	176.00 0	1.044
CuNiAl	FCC+ BCC	9.134	-8.444	1339.7 23	1.449	13.912	6.157	8.00 0	1.163	6.850	133.33 3	132.00 0	0.241
CuFe0.75Ti1.125NiAl1.1 25	FCC	13.299	-19.955	1535.5 46	1.023	15.777	7.168	6.97 5	1.194	6.378	139.50 0	131.35 0	0.259
FeMnNi	FCC	9.134	-4.444	1686.0 00	3.465	15.434	3.929	8.33 3	1.095	8.073	203.00 0	156.66 7	0.592
FeCoNiCrMn	FCC	13.381	-4.160	1801.2 00	5.794	13.836	3.269	8.00 0	1.096	8.064	219.40 0	162.00 0	1.252
Hf0.5Nb0.5Ta0.5Ti1.5Zr	BCC	12.423	-1.500	2328.1 25	19.28 1	11.169	4.788	4.25 0	1.132	8.145	106.62 5	119.00 0	0.542
HfMo0.75NbTaTiZr	BCC	14.855	-1.301	2571.6 52	29.37 3	26.209	5.653	4.60 9	1.191	9.957	139.08 7	144.95 7	0.465
HfMoNbTaTiZr	BCC	14.897	-1.889	2585.1 67	20.38 8	28.440	5.783	4.66 7	1.191	9.967	147.00 0	148.50 0	0.445
HfMoNbZrTi	BCC	13.381	-3.040	2444.2 00	10.75 8	30.955	6.097	4.60 0	1.190	8.620	139.20 0	138.20 0	0.360
HfMoTaTiZr	BCC	13.381	-3.360	2552.2 00	10.16 4	31.123	6.088	4.60 0	1.190	10.246	155.40 0	144.20 0	0.361
HfNbTaZr	BCC	11.526	3.500	2668.5 00	8.787	12.316	5.363	4.50 0	1.132	11.268	109.25 0	137.75 0	0.401
Mn2Cr2Fe2Ni2Cu	FCC	13.145	2.568	1759.3	9.006	14.237	3.369	8.11	1.096	7.974	211.77	155.55	1.158

				00				1			8	6	
Mn2CrFe2NiCu2	FCC+ BCC	12.966	3.125	1660.4 25	6.889	14.551	3.381	8.50 0	1.096	8.078	194.62 5	150.00 0	1.134
Mn2CrFeNi2Cu	FCC	12.885	0.735	1691.8 14	29.67 1	15.477	3.568	8.42 9	1.096	8.100	202.28 6	152.85 7	1.012
MnCr2Fe2Ni2Cu2	FCC+ BCC	13.145	4.741	1741.3 78	4.829	12.799	2.629	8.55 6	1.096	8.143	204.22 2	157.77 8	1.902
MnCr2Fe2NiCu	FCC+ BCC	12.885	5.061	1798.1 00	4.578	12.870	2.900	8.00 0	1.096	7.919	215.42 9	157.14 3	1.532
MnCrFe1.5Ni0.5Al0.3	BCC	12.319	-6.501	1758.0 33	3.332	12.969	4.703	7.18 6	1.168	7.373	212.67 4	150.65 1	0.557
MnCrFe1.5Ni0.5Al0.5	BCC	12.662	-8.049	1721.3 86	2.708	12.876	5.163	7.00 0	1.168	7.164	206.33 3	147.33 3	0.475
MnCrFe2Ni2Cu2	FCC	12.966	5.250	1686.5 50	4.165	12.604	2.748	8.87 5	1.096	8.263	194.87 5	157.50 0	1.717
MnCrFeNiCu	FCC+ BCC	13.381	2.720	1719.1 40	8.457	14.184	3.198	8.40 0	1.096	8.072	203.60 0	154.00 0	1.309
MnCrFeNiCuAl	BCC	14.897	-5.111	1588.1 95	4.629	14.256	5.388	7.50 0	1.169	7.175	181.33 3	141.00 0	0.513
MoNbTiV	BCC	11.526	-2.750	2442.5 00	10.23 7	24.894	4.076	5.00 0	1.120	7.351	169.50 0	167.50 0	0.694
Mo0.3NbTiVZr	BCC	12.825	-3.202	2295.5 35	9.195	19.732	7.007	4.60 5	1.238	6.689	119.93 0	134.88 4	0.261
Mo0.5NbTiVZr	BCC	13.145	-3.556	2322.2 22	8.585	22.809	6.969	4.66 7	1.238	6.845	129.22 2	139.11 1	0.271
Mo0.7NbTiVZr	BCC	13.308	-3.839	2346.6 38	8.135	25.058	6.926	4.72 3	1.238	6.988	137.72 3	142.97 9	0.277
Mo1.3NbTiVZr	BCC	13.330	-4.386	2408.8 30	7.321	29.155	6.775	4.86 8	1.238	7.352	159.37 7	152.83 0	0.290
Mo1.5NbTiVZr	BCC	13.254	-4.496	2426.5 45	7.154	29.993	6.721	4.90 9	1.238	7.455	165.54 5	155.63 6	0.293
Mo1.7NbTiVZr	BCC	13.154	-4.580	2443.0 18	7.017	30.663	6.665	4.94 7	1.238	7.551	171.28 1	158.24 6	0.296
Mo2NbTiVZr	BCC	12.976	-4.667	2465.6 67	6.856	31.425	6.582	5.00 0	1.238	7.684	179.16 7	161.83 3	0.300
MoCrFeNiCu	FCC	13.381	4.640	1994.5 40	5.752	16.117	3.580	8.20 0	1.107	8.626	229.80 0	176.00 0	1.044

MoNbTiV0.25Zr	BCC	12.708	-4.595	2414.2 94	6.677	29.786	6.316	4.76 5	1.238	7.371	152.94 1	146.11 8	0.319
MoNbTiV0.50Zr	BCC	13.145	-4.444	2401.4 44	7.103	28.952	6.554	4.77 8	1.238	7.300	151.55 6	146.88 9	0.306
MoNbTiV0.75Zr	BCC	13.332	-4.299	2389.9 47	7.411	28.186	6.728	4.78 9	1.238	7.237	150.31 6	147.57 9	0.295
MoNbTiV1.0Zr	BCC	13.381	-4.160	2379.6 00	7.654	27.477	6.853	4.80 0	1.238	7.181	149.20 0	148.20 0	0.285
MoNbTiV1.5Zr	BCC	13.254	-3.901	2361.7 27	8.024	26.205	7.006	4.81 8	1.238	7.083	147.27 3	149.27 3	0.270
MoNbTiV2.0Zr	BCC	12.976	-3.667	2346.8 33	8.305	25.096	7.071	4.83 3	1.238	7.001	145.66 7	150.16 7	0.260
MoNbTiV3.0Zr	BCC	12.264	-3.265	2323.4 29	8.726	23.243	7.059	4.85 7	1.238	6.873	143.14 3	151.57 1	0.246
MoNbTiZr	BCC	11.526	-4.750	2428.7 50	5.893	30.695	5.988	4.75 0	1.192	7.450	154.50 0	145.25 0	0.321
NbTaVW	BCC	11.526	-4.250	2979.5 00	8.080	34.259	3.432	5.25 0	1.093	12.648	207.50 0	210.00 0	0.978
NbTiV0.3Mo	BCC	10.836	-2.241	2497.5 45	12.07 9	26.910	3.477	5.00 0	1.120	7.615	178.30 3	169.09 1	0.896
NbTiV0.3Mo0.3	BCC	10.254	-1.124	2390.2 69	21.80 1	18.881	3.398	4.73 1	1.120	6.920	137.73 1	152.69 2	0.888
NbTiV0.3Mo0.5	BCC	10.662	-1.582	2426.3 93	16.35 6	22.515	3.449	4.82 1	1.120	7.154	151.39 3	158.21 4	0.896
NbTiV0.3Mo0.7	BCC	10.827	-1.911	2457.7 00	13.92 3	24.808	3.473	4.90 0	1.120	7.357	163.23 3	163.00 0	0.897
NbTiV0.3Mo1.3	BCC	10.696	-2.438	2530.7 50	11.10 2	28.099	3.458	5.08 3	1.120	7.831	190.86 1	174.16 7	0.895
NbTiV0.3Mo1.5	BCC	10.559	-2.521	2549.9 74	10.68 1	28.583	3.436	5.13 2	1.120	7.955	198.13 2	177.10 5	0.894
NbTiV0.3Zr	BCC	10.836	-1.873	2264.8 18	13.10 1	11.748	6.005	4.39 4	1.237	6.494	99.212	120.90 9	0.301
NbTiV2Zr	BCC	11.076	-2.720	2237.0 00	9.109	11.289	7.481	4.60 0	1.237	6.361	109.00 0	134.20 0	0.198
NbTiVZr	BCC	11.526	-2.500	2250.5 00	10.37 5	11.715	7.048	4.50 0	1.237	6.426	104.25 0	127.75 0	0.232
Ti0.5Co1.5CrFeNi1.5	FCC	12.858	-16.364	1855.5	1.458	12.187	4.885	8.09	1.197	8.012	211.18	168.18	0.539

				45				1			2	2	
Ti0.5Co1.5CrFeNi1.5Mo 0.1	FCC	13.374	-16.027	1874.1 25	1.564	12.945	4.938	8.05 4	1.196	8.051	213.28 6	169.28 6	0.548
Ti0.5Co1.5CrFeNiAl	FCC+ BCC	14.534	-21.611	1712.4 95	1.152	13.256	6.536	7.08 3	1.195	7.050	188.58 3	151.83 3	0.340
Ti0.5Co2CrFeNiAl	FCC+ BCC	14.232	-20.355	1716.7 65	1.200	13.089	6.364	7.23 1	1.195	7.193	190.15 4	154.00 0	0.351
Ti0.5Co3CrFeNiAl	FCC+ BCC	13.483	-18.204	1723.5 96	1.277	12.694	6.050	7.46 7	1.195	7.422	192.66 7	157.46 7	0.368
Ti0.5CoCrFeNiCu0.75Al 0.25	FCC	15.547	-15.645	1765.2 99	1.754	12.737	5.459	8.00 0	1.196	7.735	194.90 9	158.00 0	0.522
TiVNbMo	BCC	11.526	-2.750	2442.5 00	10.23 7	24.894	4.076	5.00 0	1.120	7.351	169.50 0	167.50 0	0.694
TiCoCrFeNiCuAlIV	FCC+ BCC	17.288	-13.938	1737.7 71	2.156	14.027	6.338	7.00 0	1.196	6.895	167.87 5	147.00 0	0.430
TiCr0.5FeNiCuAl	FCC+ BCC	14.697	-13.620	1611.1 22	1.739	14.909	7.099	7.09 1	1.195	6.646	157.54 5	137.45 5	0.292
TiCr1.5FeNiCuAl	FCC+ BCC	14.784	-13.538	1698.6 42	1.855	14.086	6.905	6.92 3	1.195	6.730	176.23 1	140.92 3	0.310
TiCr2FeNiCuAl	FCC+ BCC	14.532	-13.306	1733.0 24	1.893	13.711	6.794	6.85 7	1.195	6.763	183.57 1	142.28 6	0.315
TiCr3FeNiCuAl	FCC+ BCC	13.863	-12.688	1788.8 96	1.955	13.033	6.566	6.75 0	1.195	6.816	195.50 0	144.50 0	0.322
TiCrFeNiCuAl	FCC+ BCC	14.897	-13.667	1658.5 28	1.808	14.485	7.009	7.00 0	1.195	6.692	167.66 7	139.33 3	0.303

Data S3 The data source for Figure 2

MPEAs	Dimension 1	Dimension 2	Phase
Al0.10CoCrFeMnNi	-11.624	-5.184	FCC
Al0.20CoCrFeMnNi	-11.219	-4.956	FCC
Al0.25CoCrCu0.5FeNiTi0.5	-8.205	6.300	FCC
Al0.25CoCrCu0.75FeNiTi0.5	-8.600	6.690	FCC
Al0.25CoCrFeNi	-12.095	-4.180	FCC
Al0.25CoFeNi	-9.482	-5.438	FCC
Al0.25MoNbTiV	21.718	9.960	BCC
Al0.25NbTaTiV	17.818	5.381	BCC
Al0.2Co1.5CrFeNi1.5Ti0.5	-10.670	-0.585	FCC
Al0.375CoCrFeNi	-10.904	-3.390	FCC
Al0.38CoCrFeMnNi	-9.177	0.453	FCC
Al0.3CoCrCuFe	-10.228	-9.226	FCC
Al0.3CrFe1.5MnNi0.5	-7.177	-2.485	FCC+BCC
Al0.3HfNbTaTiZr	18.285	6.727	BCC
Al0.3NbTa0.8Ti1.4V0.2Zr1.3	16.587	7.763	BCC
Al0.3NbTaTi1.4Zr1.3	17.216	6.605	BCC
Al0.43CoCrFeMnNi	-9.053	0.814	FCC+BCC
Al0.49CoCrFeMnNi	-8.843	1.194	FCC+BCC
Al0.4CrCuFeNi2	-9.754	-9.297	FCC
Al0.4Hf0.6NbTaTiZr	17.874	6.637	BCC
Al0.56CoCrFeMnNi	-8.647	1.639	FCC+BCC
Al0.5CoCrCu0.5FeNiTi0.5	-6.907	6.950	FCC+BCC
Al0.5CoCrCuFe	-10.541	-13.273	FCC
Al0.5CoCrCuFeNi	-8.754	-12.230	FCC
Al0.5CoCrCuFeNiTi	-5.306	7.953	FCC+BCC
Al0.5CoCrCuFeNiTi0.2	-5.348	-10.440	FCC
Al0.5CoCrCuFeNiTi0.4	-8.541	7.326	FCC
Al0.5CoCrCuFeNiTi0.6	-7.407	7.529	FCC+BCC
Al0.5CoCrCuFeNiTi0.8	-6.290	7.697	FCC+BCC
Al0.5CoCrCuFeNiTi1.2	-4.485	8.073	FCC+BCC
Al0.5CoCrCuFeNiTi1.4	-3.846	7.908	FCC+BCC
Al0.5CoCrCuFeNiTi1.6	-3.267	7.766	FCC+BCC
Al0.5CoCrCuFeNiTi1.8	-2.738	7.849	FCC+BCC
Al0.5CoCrCuFeNiTi2	-2.380	7.632	FCC+BCC
Al0.5CoCrCuFeNiV0.2	-7.689	-12.417	FCC
Al0.5CoCrCuFeNiV0.4	-6.791	-12.967	FCC+BCC
Al0.5CoCrCuFeNiV0.6	-6.248	-13.582	FCC+BCC
Al0.5CoCrCuFeNiV0.8	-6.397	-14.258	FCC+BCC
Al0.5CoCrCuFeNiV1.0	-5.776	-14.373	FCC+BCC
Al0.5CoCrCuFeNiV1.2	-6.743	-15.179	BCC
Al0.5CoCrCuFeNiV1.4	-5.298	-14.877	BCC

Al0.5CoCrCuFeNiV1.6	-5.944	-15.730	BCC
Al0.5CoCrCuFeNiV1.8	-6.228	-16.277	BCC
Al0.5CoCrCuFeNiV2.0	-5.631	-16.452	BCC
Al0.5CoCrFeNi	-10.100	-2.566	FCC+BCC
Al0.5CoFeNi	-8.894	-4.752	FCC+BCC
Al0.5CrCuFeNi2	-9.650	-8.717	FCC
Al0.5CrFe1.5MnNi0.5	-6.445	-2.000	BCC
Al0.5HfNbTaTiZr	17.947	6.873	BCC
Al0.5MoNbTiV	21.368	9.559	BCC
Al0.5NbTa0.8Ti1.5V0.2Zr	16.515	7.468	BCC
Al0.5NbTaTiV	17.457	5.438	BCC
Al0.62CoCrFeMnNi	-8.416	2.001	FCC+BCC
Al0.68CoCrFeMnNi	-8.303	2.411	FCC+BCC
Al0.6CrCuFeNi2	-9.393	-8.315	FCC
Al0.75CoCrCu0.25FeNiTi0.5	-4.682	7.094	FCC+BCC
Al0.75CoCrFeMnNi	-8.134	2.873	FCC+BCC
Al0.75CoCrFeNi	-6.377	-0.033	FCC+BCC
Al0.75CoFeNi	-12.957	0.679	FCC+BCC
Al0.75HfNbTaTiZr	17.721	7.039	BCC
Al0.75MoNbTiV	21.150	9.301	BCC
Al0.7Co0.3CrFeNi	-5.278	-0.380	FCC+BCC
Al0.81CoCrFeMnNi	-7.632	2.717	FCC+BCC
Al0.875CoCrFeNi	-5.466	0.480	FCC+BCC
Al0.88CoCrFeMnNi	-7.445	3.147	FCC+BCC
Al0.8CoCrCuFe	-1.931	-11.425	FCC+BCC
Al0.8CoCrCuFeNi	-4.141	-9.703	FCC+BCC
Al0.8CrCuFeNi2	0.349	-9.805	FCC
Al0.95CoCrFeMnNi	-7.054	3.227	FCC+BCC
Al1.125CuFe0.75NiTi1.125	3.615	4.443	FCC
Al1.25CoCrFeMnNi	-6.171	3.617	BCC
Al1.25CoCrFeNi	-2.964	1.634	BCC
Al1.2CrCuFeNi2	1.827	-8.975	FCC+BCC
Al1.3CoCrCuFe	2.362	-6.020	FCC+BCC
Al1.3CoCrCuFeNi	-1.409	-6.750	FCC+BCC
Al1.5CoCrCuFe	3.138	-4.591	FCC+BCC
Al1.5CoCrCuFeNi	-0.654	-5.583	FCC+BCC
Al1.5CoCrFeNi	-1.577	1.809	BCC
Al1.5CoCrFeNiTi	0.671	6.278	BCC
Al1.8CoCrCuFe	3.872	-2.957	FCC+BCC
Al1.8CoCrCuFeNi	0.543	-3.978	FCC+BCC
Al2.0CoCrCuFe	4.163	-2.170	FCC+BCC
Al2.0CrCuFeNi2	4.247	-3.557	BCC
Al2.3CoCrCuFe	4.215	-1.368	FCC+BCC

Al2.3CoCrCuFeNi	1.705	-2.416	FCC+BCC
Al2.5CoCrCuFe	4.357	-0.915	FCC+BCC
Al2.5CoCrCuFeNi	2.071	-1.886	FCC+BCC
Al2.5CoCrFeNi	2.757	1.757	BCC
Al2.8CoCrCuFe	4.204	-0.320	BCC
Al2.8CoCrCuFeNi	2.522	-1.337	BCC
Al2CoCrCuFeNi	3.615	4.443	FCC
Al2CoCrFeMo0.5Ni	1.111	-3.238	FCC+BCC
Al2CoCrFeNi	-1.380	3.755	BCC
Al2CoCrFeNiTi	1.656	1.741	BCC
Al3.0CoCrCuFe	1.126	6.116	BCC
Al3CoCrCuFeNi	4.560	-0.128	BCC
Al3CoCrFeNi	2.832	-0.955	BCC
AlCo2CrFeMo0.5Ni	3.535	1.686	BCC
AlCoCrCuFe	-10.014	2.009	FCC+BCC
AlCoCrCuFeMnNi	1.001	-7.083	FCC+BCC
AlCoCrCuFeNi	-4.387	-7.631	FCC+BCC
AlCoCrCuFeNiTi	-2.948	-8.254	FCC+BCC
AlCoCrCuFeNiV	-3.485	8.485	FCC+BCC
AlCoCrCuNiTi	-3.432	-13.893	FCC+BCC
AlCoCrFeMo0.1Ni	-1.486	7.187	BCC
AlCoCrFeMo0.5Ni1.5	-5.493	1.635	BCC
AlCoCrFeMo0.5Ni2	-9.793	2.593	FCC+BCC
AlCoCrFeNb0.1Ni	-10.095	2.049	FCC+BCC
AlCoCrFeNi	-4.618	1.879	BCC
AlCoCrFeNiNb0.1	-4.558	0.884	BCC
AlCoCrFeNiSi	-4.617	1.880	BCC
AlCoCrFeNiSi0.2	0.890	8.497	BCC
AlCoCrFeNiSi0.4	0.243	9.791	BCC
AlCoCrFeNiSi0.6	0.249	9.444	BCC
AlCoCrFeNiTi	0.407	9.002	BCC
AlCoCrFeNiTi0.5	-0.205	6.040	BCC
AlCoCuFeNi	-2.471	5.620	BCC
AlCoCuFeNiSi	1.801	-9.901	FCC+BCC
AlCoCuFeNiTi	3.529	5.515	FCC+BCC
AlCoCuFeNiZr	3.028	3.912	FCC+BCC
AlCoFeNi	3.026	7.339	FCC+BCC
AlCoFeNiTiVZr	5.988	1.609	BCC
AlCr0.5NbTiV	2.691	7.658	BCC
AlCrCuFeNi	15.397	5.984	BCC
AlCrCuFeNi0.6	1.216	-7.789	FCC+BCC
AlCrCuFeNi0.8	1.738	-6.822	FCC+BCC
AlCrCuFeNi1.2	1.629	-7.301	FCC+BCC

AlCrCuFeNi1.4	0.986	-8.241	FCC+BCC
AlCrCuFeNi2	0.995	-8.664	FCC+BCC
AlCrFeNi	0.979	-9.411	FCC+BCC
AlCrFeNiMo0.2	-1.564	0.266	BCC
AlCrFeNiMo0.5	-2.855	0.282	BCC
AlCuFeNiTi	-3.552	-0.308	BCC
AlCuNiTi	3.121	4.319	FCC
AlMo0.5NbTa0.5TiZr	4.464	3.917	FCC
AlMoNbTiV	18.951	8.346	BCC
AlNb1.5Ta0.5Ti1.5Zr0.5	21.003	9.136	BCC
AlNbTaTiV	16.169	5.791	BCC
AlNbTiV	16.858	5.505	BCC
Co0.5CrFeNiCuAl	15.577	5.593	BCC
Co1.5CrFeNi1.5Ti0.5	-1.985	-7.476	FCC+BCC
CoCr0.5FeNiCuAl	-11.093	-1.631	FCC
CoCrCuFeNiTi	-2.501	-7.134	FCC+BCC
CoCrCuFeNiTi0.5	-7.972	6.757	FCC
CoCrFe0.5NiCuAl	-6.293	-10.479	FCC
CoCrFeMnNi	-2.083	-8.574	FCC+BCC
CoCrFeMnNiV0.25	-14.923	-9.281	FCC
CoCrFeMnNiV0.5	-15.513	-9.447	FCC
CoCrFeNi0.5CuAl	-15.722	-9.468	FCC
CoCrFeNiAl	-1.766	-8.031	FCC+BCC
CoCrFeNiAl0.25	-4.558	0.884	BCC
CoCrFeNiAl0.375	-12.045	-3.942	FCC
CoCrFeNiAl0.3Mo0.1	-10.988	-3.097	FCC
CoCrFeNiAl0.5	-11.566	-3.537	FCC
CoCrFeNiAl0.75	-10.101	-2.376	FCC+BCC
CoCrFeNiAl0.875	-6.343	0.147	FCC+BCC
CoCrFeNiAl1.25	-5.517	0.623	FCC+BCC
CoCrFeNiAl1.5	-3.079	1.522	BCC
CoCrFeNiAl2	-1.700	1.720	BCC
CoCrFeNiAl2.5	1.618	1.516	BCC
CoCrFeNiAl3	2.741	1.339	BCC
CoCrFeNiCu0.25Al	3.564	1.232	BCC
CoCrFeNiCu0.25Al0.75	-1.970	-9.582	BCC
CoCrFeNiCu0.5Al	-3.045	-10.183	FCC+BCC
CoCrFeNiCu0.5Al0.5	-2.366	-9.070	BCC
CoCrFeNiCu0.75Al0.25	-6.954	-11.183	FCC
CoCrFeNiCuAl	-10.164	-11.092	FCC
CoCrFeNiCuAl0.3	-2.948	-8.254	FCC+BCC
CoCrFeNiCuAl0.5	-9.931	-11.154	FCC
CoCrFeNiCuAl0.5V0.2	-6.890	-11.728	FCC

CoCrFeNiCuAl0.5V0.4	-7.178	-13.628	FCC
CoCrFeNiCuAl0.5V1.2	-7.103	-14.271	FCC+BCC
CoCrFeNiCuAl0.5V1.4	-6.146	-15.021	FCC+BCC
CoCrFeNiCuAl0.5V1.6	-6.608	-15.676	FCC+BCC
CoCrFeNiCuAl0.5V1.8	-5.548	-15.391	FCC+BCC
CoCrFeNiCuAl0.5V2	-5.005	-15.576	FCC+BCC
CoCrFeNiCuAl0.8	-5.167	-16.127	FCC+BCC
CoCrFeNiCuAl1.3	-3.952	-9.198	FCC+BCC
CoCrFeNiCuAl1.5	-1.293	-7.273	FCC+BCC
CoCrFeNiCuAl1.8	-0.673	-6.301	FCC+BCC
CoCrFeNiCuAl2	0.590	-4.893	FCC+BCC
CoCrFeNiCuAl2.3	1.436	-4.272	FCC+BCC
CoCrFeNiCuAl2.5	2.153	-3.585	BCC
CoCrFeNiCuAl2.8	2.577	-3.146	BCC
CoCrFeNiCuAl3	2.982	-2.575	BCC
CoCrFeNiCuAlSi	3.290	-2.123	BCC
CoCrFeNiCuAlIV	-0.735	9.305	FCC+BCC
CoCrFeNiMnCu	-3.432	-13.893	FCC+BCC
CoCrFeNiMo0.3	-14.922	-9.276	FCC
CoCrFeNiPd	-12.984	-12.326	FCC
CoCrFeNiPd2	-16.627	-10.858	FCC
CoCrFeNiTi	-15.088	-6.145	FCC
CoCrMnNi	-15.101	-5.968	FCC
CoCrNiCu0.5Al	-4.377	3.540	FCC
CoCrNiCuAl	-13.996	-8.023	FCC
CoCuFeMnNi	2.465	-8.416	BCC
CoCuFeMnNiSn0.03	1.645	-8.800	FCC+BCC
CoCuFeNiSn0.02	-13.404	-11.628	FCC
CoCuNiAl	-7.804	-9.600	FCC
CoFeMnNi	-7.989	-9.267	FCC
CoFeNiCuV	-13.976	1.712	FCC+BCC
CoFeNiSi0.25	-13.770	-7.959	FCC
CoFeNiV	-16.345	-12.313	FCC
CoMnNi	-17.446	-11.756	FCC
CrCuFeMnNi	-17.335	-11.559	FCC
CrCuFeMoNi	-12.820	-7.153	FCC
CuNiAl	-14.048	-10.876	FCC+BCC
CuFe0.75Ti1.125NiAl1.125	-16.162	-8.020	FCC
FeMnNi	6.799	-0.273	FCC+BCC
FeCoNiCrMn	-12.789	-7.152	FCC
Hf0.5Nb0.5Ta0.5Ti1.5Zr	17.606	8.451	BCC
HfMo0.75NbTaTiZr	21.271	14.502	BCC
HfMoNbTaTiZr	21.003	14.287	BCC

HfMoNbZrTi	20.079	13.011	BCC
HfMoTaTiZr	20.328	13.621	BCC
HfNbTaZr	19.198	6.319	BCC
Mn2Cr2Fe2Ni2Cu	-14.056	-10.210	FCC
Mn2CrFe2NiCu2	-13.547	-10.632	FCC+BCC
Mn2CrFeNi2Cu	-11.183	-13.261	FCC
MnCr2Fe2Ni2Cu2	-15.271	-11.541	FCC+BCC
MnCr2Fe2NiCu	-15.048	-10.768	FCC+BCC
MnCrFe1.5Ni0.5Al0.3	-7.173	-2.386	BCC
MnCrFe1.5Ni0.5Al0.5	-6.359	-1.851	BCC
MnCrFe2Ni2Cu2	-14.891	-11.725	FCC
MnCrFeNiCu	-14.048	-10.876	FCC+BCC
MnCrFeNiCuAl	-1.814	-6.249	BCC
MoNbTiV	17.183	10.919	BCC
Mo0.3NbTiVZr	17.540	11.525	BCC
Mo0.5NbTiVZr	17.630	12.156	BCC
Mo0.7NbTiVZr	18.236	13.452	BCC
Mo1.3NbTiVZr	18.956	13.342	BCC
Mo1.5NbTiVZr	19.013	13.703	BCC
Mo1.7NbTiVZr	18.714	14.116	BCC
Mo2NbTiVZr	-16.162	-8.020	FCC
MoCrFeNiCu	22.448	10.660	BCC
MoNbTiV0.25Zr	19.223	12.650	BCC
MoNbTiV0.50Zr	18.987	12.322	BCC
MoNbTiV0.75Zr	18.594	12.676	BCC
MoNbTiV1.0Zr	18.145	12.842	BCC
MoNbTiV1.5Zr	17.714	12.787	BCC
MoNbTiV2.0Zr	18.294	12.048	BCC
MoNbTiV3.0Zr	18.363	11.558	BCC
MoNbTiZr	19.821	12.027	BCC
NbTaVW	22.448	10.660	BCC
NbTiV0.3Mo	24.658	10.324	BCC
NbTiV0.3Mo0.3	23.173	10.867	BCC
NbTiV0.3Mo0.5	22.908	12.180	BCC
NbTiV0.3Mo0.7	22.748	11.712	BCC
NbTiV0.3Mo1.3	22.781	11.285	BCC
NbTiV0.3Mo1.5	23.434	10.508	BCC
NbTiV0.3Zr	23.683	10.549	BCC
NbTiV2Zr	16.347	9.493	BCC
NbTiVZr	16.233	9.953	BCC
Ti0.5Co1.5CrFeNi1.5	16.328	9.772	BCC
Ti0.5Co1.5CrFeNi1.5Mo0.1	-11.484	-1.018	FCC
Ti0.5Co1.5CrFeNiAl	-11.396	-0.853	FCC

Ti0.5Co2CrFeNiAl	-2.983	5.267	FCC+BCC
Ti0.5Co3CrFeNiAl	-3.318	4.862	FCC+BCC
Ti0.5CoCrFeNiCu0.75Al0.25	-4.000	3.770	FCC+BCC
TiVNbMo	-7.104	5.933	FCC
TiCoCrFeNiCuAlV	-3.835	9.295	FCC+BCC
TiCr0.5FeNiCuAl	-0.649	6.979	FCC+BCC
TiCr1.5FeNiCuAl	-1.600	6.283	FCC+BCC
TiCr2FeNiCuAl	-1.592	5.460	FCC+BCC
TiCr3FeNiCuAl	-2.374	3.170	FCC+BCC
TiCrFeNiCuAl	-1.282	6.826	FCC+BCC

Data S4. The data source of the yield strengths collected from experiments for various MPEAs. (separate file)

The data set includes 53 entries derived from the experiments in the prior research. For each entry, we list the experimental and predicted yield strengths, the deviation between experiments and model prediction, and the corresponding references.

MPEAs	Experimental yield stress (MPa)	Calculated yield stress (MPa)	Deviations (%)	References
Al0.25CoFeNi	158	153	3.164556962	T.T. Zuo, R.B. Li, X.J. Ren, Y. Zhang, Effects of Al and Si addition on the structure and properties of CoFeNi equal atomic ratio alloy, <i>J. Magn. Magn. Mater.</i> 371 (2014) 60–68.
Al0.38CoCrFeMnNi	244	208	14.75409836	He, J.Y., Liu, W.H., Wang, H., Wu, Y., Liu, X.J., Nieh, T.G., Lu, Z.P., 2014. Effects of Al addition on structural evolution and tensile properties of the FeCoNiCrMn high-entropy alloy system. <i>Acta Mater.</i> 62, 105-113.
Al0.3HfNbTaTiZr	1188	916	22.8956229	C.-M. Lin, C.-C. Juan, C.-H. Chang, C.-W. Tsai, J.-W. Yeh, Effect of Al addition on mechanical properties and microstructure of refractory AlxHfNbTaTiZr alloys, <i>J. Alloy. Compd.</i> 624 (2015) 100–107
Al0.75HfNbTaTiZr	1514	1511	0.198150594	
AlNb1.5Ta0.5Ti1.5Zr0.5	1280	1137	11.171875	O.N. Senkov, C. Woodward, D.B. Miracle, Microstructure and properties of aluminum-containing refractory high entropy alloys, <i>JOM</i> 66 (10) (2014) 2030–2042.
AlMo0.5NbTa0.5TiZr	2000	1966	1.7	
Al0.3NbTa0.8Ti1.4V0.2Zr1.3	1965	2010	2.290076336	

Al0.5CoCrCuFeNi	388	363	6.443298969	Chen, M.R., Lin, S.J., Yeh, J.W., Chen, S.K., Huang, Y.S., Chuang, M.H., 2006. Effect of vanadium addition on the microstructure, hardness, and wear resistance of Al0.5CoCrCuFeNi high-entropy alloy. Metall. Mater. Trans. A 37, 1363-1369.
Al0.25MoNbTiV	1250	1230	1.6	Chen, S.Y., Yang, X., Dahmen, K.A., Liaw, P.K., Zhang, Y., 2014. Microstructures and crackling noise of Al _x NbTiMoV high entropy alloys. Entropy 16, 870-884.
Al0.5MoNbTiV	1625	1364	16.06153846	
Al0.75MoNbTiV	1260	1213	3.73015873	
AlMoNbTiV	1375	1413	2.763636364	
AlCoCrFeMo0.1Ni	1804	1672	7.317073171	J.M. Zhu, H.M. Fu, H.F. Zhang, A.M. Wang, H. Li, Z.Q. Hua, Microstructures and compressive properties of multicomponent AlCoCrFeNiMox alloys, Mater. Sci. Eng. A 527 (2010) 6975–6979
AlCoCrFeNb0.1Ni	1641	1643	0.121876904	S.G. Ma, Y. Zhang, Effect of Nb addition on the microstructure and properties of AlCoCrFeNi high-entropy alloy, Mater. Sci. Eng. A 532 (2012) 480–486
AlCoCrFeNiTi	1860	1595	14.24731183	Y.J. Zhou, Y. Zhang, Y.L. Wang, G.L. Chen, Solid solution alloys of AlCoCrFeNiTix with excellent room-temperature mechanical properties, Cit.: Appl.

				Phys. Lett. 90 (2007) 181904.
AlCoCrFeNiTi0.5	2260	2058	8.938053097	F.J. Wang, Y. Zhang, G.L. Chen, Atomic packing efficiency and phase transition in a high entropy alloy, <i>J. Alloy. Compd.</i> 478 (2009) 321–324
AlCuFeNiTi	1074	899	16.29422719	Fazakas, E., Zadorozhnyy, V., Louguine-Luzgin, D.V., 2015. Effect of iron content on the structure and mechanical properties of Al25Ti25Ni25Cu25 and (AlTi) _{60-x} Ni ₂₀ Cu ₂₀ Fex (x ¼15, 20) high-entropy alloys. <i>Appl. Surf. Sci.</i> 358, 549-555.
AlCuNiTi	300	281	6.333333333	
CoCrCuFeNiTi	1272	944	25.78616352	Wang, X.F., Zhang, Y., Qiao, Y., Chen, G.L., 2007. Novel microstructure and properties of multicomponent CoCrCuFeNiTix alloys. <i>Intermetallics</i> 15, 357-362.
CoCrCuFeNiTi0.5	700	545	22.14285714	
CoCrFeMnNi	230	205	10.86956522	Stepanov, N.D., Shaysultanov, D.G., Salishchev, G.A., Tikhonovsky, M.A., Oleynik, E.E., Tortika, A.S., Senkov, O.N., 2015. Effect of V content on microstructure and mechanical properties of the CoCrFeMnNiVx high entropy alloys. <i>J. Alloy. Compd.</i> 628, 170-185.
CoCrFeMnNiV0.25	200	190	5	
CoCrFeNi	148	176	18.91891892	Wu, Z., Bei, H., Pharr, G.M., George, E.P., 2014. Temperature dependence of the mechanical properties of equiatomic solid solution alloys with face-centered

CoCrMnNi	282	260	7.80141844	cubic crystal structures. Acta Mater. 81, 428-441.
FeMnNi	221	210	4.977375566	
Hf0.5Nb0.5Ta0.5Ti1.5Zr	903	979	8.416389812	Sheikh, S., Shafeie, S., Hu, Q., Ahlstrom, J., Persson, C., Vesely, J., Zyka, J., Klement, U., Guo, S., 2016. Alloy design for intrinsically ductile refractory high-entropy alloys. J. Appl. Phys. 120, 164902.
HfMo0.25NbTaTiZr	1112	1192	7.194244604	
HfMo0.5NbTaTiZr	1317	1327	0.759301443	Juan, C.-C., Tseng, K.-K., Hsu, W.-L., Tsai, M.-H., Tsai, C.-W., Lin, C.-M., Chen, S.-K., Lin, S.-J., Yeh, J.-W., 2016. Solution strengthening of ductile refractory HfMoNbTaTiZr high-entropy alloys. Mater. Lett. 175, 284-287.
HfMo0.75NbTaTiZr	1373	1412	2.840495266	
HfMoNbTaTiZr	1512	1491	1.388888889	
HfNbTaTiZr	1015	1026	1.083743842	
HfMoNbZrTi	1803	2030	12.59012757	Guo, N.N., Wang, L., Luo, L.S., Li, X.Z., Su, Y.Q., Guo, J.J., Fu, H.Z., 2015. Microstructure and mechanical properties of refractory MoNbHfZrTi high-entropy alloy. Mater. Des. 81, 87-94.
Mo0.5NbTiVZr	1473	1725	17.10794297	Y.D. Wu, Y.H. Cai, X.H. Chen, T. Wang, J.J. Si, L. Wang, Y.D. Wang, X.D. Hui, Phase composition and solid

Mo0.7NbTiVZr	1706	1730	1.406799531	solution strengthening effect in TiZrNbMoV high-entropy alloys, Mater. Des. 83 (2015) 651–660.
Mo1.3NbTiVZr	1496	1760	17.64705882	
Mo1.5NbTiVZr	1603	1768	10.29320025	
Mo1.7NbTiVZr	1645	1773	7.781155015	
Mo2NbTiVZr	1765	1780	0.849858357	
MoNbTaV	1525	1546	1.37704918	
MoNbTaW	1058	1115	5.387523629	Senkov, O.N., Wilks, G.B., Scott, J.M., Miracle, D.B., 2011b. Mechanical properties of Nb25Mo25Ta25W25 and V20Nb20Mo20Ta20W20 refractory high entropy alloys. <i>Intermetallics</i> 19, 698-706.
MoNbTiV0.25Zr	1776	2014	13.4009009	Y.D. Wu, Y.H. Cai, X.H. Chen, T. Wang, J.J. Si, L. Wang, Y.D. Wang, X.D. Hui, Phase composition and solid solution strengthening effect in TiZrNbMoV high-entropy alloys, Mater. Des. 83 (2015) 651–660.
MoNbTiV0.50Zr	1647	1880	14.14693382	
MoNbTiV0.75Zr	1708	1859	8.840749415	
MoNbTiV1.0Zr	1786	1746	2.239641657	

MoNbTiV1.5Zr	1735	1550	10.66282421	
MoNbTiV2.0Zr	1538	1466	4.681404421	
MoNbTiV3.0Zr	1418	1347	5.007052186	
NbTiVZr	1104	1231	11.50362319	
MoNbTiVZr	1779	1618	9.050028106	
MoNbTiZr	1595	1826	14.48275862	Zhang, Y., Yang, X., Liaw, P.K., 2012. Alloy design and properties optimization of high entropy alloys. <i>JOM</i> 64, 830-838.
NbTaTiV	1092	821	24.81684982	Yang, X., Zhang, Y., Liaw, P.K., 2012. Microstructure and compressive properties of NbTiVTaAlx high entropy alloys. <i>Procedia Eng.</i> 36, 292-298.
NbTaVW	1530	1719	12.35294118	Yao, H.W., Qiao, J.W., Gao, M.C., Hawk, J.A., Ma, S.G., Zhou, H.F., Zhang, Y., 2016b. NbTaV-(Ti,W) refractory high-entropy alloys: experiments and modeling. <i>Mater. Sci. Eng. A</i> 674, 203-211.
NbTiV2Zr	918	922	0.435729847	Senkov, O.N., Senkova, V., Miracle, D.B., Woodward, C., 2013. Mechanical properties of low-density, refractory multi-principal element alloys of the Cr-Nb-Ti-V-Zr system. <i>Mater. Sci. Eng. A</i> 565, 51-62.

Data S5 The “composition-phase fraction” data set in Al-Fe-Co-Cr-Ni-Mn system is established using data augment strategy.

Al(at.%)	Fe(at.%)	Co(at.%)	Cr(at.%)	Ni(at.%)	Mn(at.%)	BCC(%)	FCC(%)
8	18.4	18.4	18.4	18.4	18.4	5.77	94.23
8.26	18.348	18.348	18.348	18.348	18.348	7.03	92.97
8.47	18.306	18.306	18.306	18.306	18.306	8.3	91.7
8.68	18.264	18.264	18.264	18.264	18.264	9.38	90.62
9	18.2	18.2	18.2	18.2	18.2	11.38	88.62
9.24	18.152	18.152	18.152	18.152	18.152	13.36	86.64
9.46	18.108	18.108	18.108	18.108	18.108	15.34	84.66
9.65	18.07	18.07	18.07	18.07	18.07	16.97	83.03
9.83	18.034	18.034	18.034	18.034	18.034	18.59	81.41
10	18	18	18	18	18	20.22	79.78
10.29	17.942	17.942	17.942	17.942	17.942	21.48	78.52
10.49	17.902	17.902	17.902	17.902	17.902	22.57	77.43
10.67	17.866	17.866	17.866	17.866	17.866	23.65	76.35
10.82	17.836	17.836	17.836	17.836	17.836	24.38	75.62
11	17.8	17.8	17.8	17.8	17.8	25.64	74.36
11.17	17.766	17.766	17.766	17.766	17.766	28.7	71.3
11.31	17.738	17.738	17.738	17.738	17.738	31.59	68.41
11.43	17.714	17.714	17.714	17.714	17.714	34.11	65.89
11.54	17.692	17.692	17.692	17.692	17.692	36.45	63.55
11.69	17.662	17.662	17.662	17.662	17.662	39.51	60.49
11.83	17.634	17.634	17.634	17.634	17.634	42.04	57.96
12	17.6	17.6	17.6	17.6	17.6	45.64	54.36
12.15	17.57	17.57	17.57	17.57	17.57	51.22	48.78
12.31	17.538	17.538	17.538	17.538	17.538	57.16	42.84
12.45	17.51	17.51	17.51	17.51	17.51	62.38	37.62
12.6	17.48	17.48	17.48	17.48	17.48	67.78	32.22
12.76	17.448	17.448	17.448	17.448	17.448	73.9	26.1
12.86	17.428	17.428	17.428	17.428	17.428	77.68	22.32
13	17.4	17.4	17.4	17.4	17.4	82.72	17.28
13.23	17.354	17.354	17.354	17.354	17.354	85.78	14.22
13.42	17.316	17.316	17.316	17.316	17.316	88.85	11.15
13.59	17.282	17.282	17.282	17.282	17.282	91	9
13.75	17.25	17.25	17.25	17.25	17.25	93.53	6.47
13.88	17.224	17.224	17.224	17.224	17.224	95.52	4.48
14	17.2	17.2	17.2	17.2	17.2	96.96	3.04

Data S6 The data set includes 64 entries collected from the experiments in the previous researches, including alloy compositions, elongation and references.

Alloys	Elongation (%)	References
FeCrCuMnNi	14	Shabani, A., Toroghinejad, M. R., Shafyei, A., & Logé, R. E. (2019). Microstructure and mechanical properties of a multiphase FeCrCuMnNi high-entropy alloy. <i>Journal of Materials Engineering and Performance</i> , 28(4), 2388-2398.
CoCrFeNi	63	Liu, J., Guo, X., Lin, Q., He, Z., An, X., Li, L., ... & Zhang, Y. (2019). Excellent ductility and serration feature of metastable CoCrFeNi high-entropy alloy at extremely low temperatures. <i>Science China Materials</i> , 62(6), 853-863.
Al0.20CoCrFeMnNi	56	
Al0.38CoCrFeMnNi	45	
Al0.43CoCrFeMnNi	35	
Al0.49CoCrFeMnNi	29	
Al0.56CoCrFeMnNi	16	
Al0.62CoCrFeMnNi	5	
CoCrMnNi	44	
CoCrNi	60	
CoFeMnNi	41	
CoFeNi	31	
Al0.16CoCrFeNiTi0.08	70	He, J. Y., Wang, H., Huang, H. L., Xu, X. D., Chen, M. W., Wu, Y., ... & Lu, Z. P. (2016). A precipitation-hardened high-entropy alloy with outstanding tensile properties. <i>Acta Materialia</i> , 102, 187-196.
AlCrCoFeNi2.1	16.5	
AlCrCoFeNi2.2	20	
AlCrCoFeNi2	16.5	Lu, Y., Gao, X., Jiang, L., Chen, Z., Wang, T., Jie, J., ... & Li, T. (2017). Directly cast bulk eutectic and near-eutectic high entropy alloys with balanced strength and ductility in a wide temperature range. <i>Acta materialia</i> , 124, 143-150.
FeCoNiCrTi0.2	36	Tong, Y., Chen, D., Han, B., Wang, J., Feng, R., Yang, T., ... & Kai, J. J. (2019). Outstanding tensile properties of a precipitation-strengthened FeCoNiCrTi0.2 high-entropy alloy at room and cryogenic temperatures. <i>Acta Materialia</i> , 165, 228-240.
Al0.1CoCrFeNi	30.3	Wu, S. W., Wang, G., Wang, Q., Jia, Y. D., Yi, J., Zhai, Q. J., ... & Zhang, T. Y. (2019). Enhancement of strength-ductility trade-off in a high-entropy alloy through a heterogeneous structure. <i>Acta Materialia</i> , 165, 444-458.

Co0.5CrNi	64	Yoshida, S., Ikeuchi, T., Bhattacharjee, T., Bai, Y., Shibata, A., & Tsuji, N. (2019). Effect of elemental combination on friction stress and Hall-Petch relationship in face-centered cubic high/medium entropy alloys. <i>Acta Materialia</i>, 171, 201-215.
CoNiCr0.5	36	
CoMnNi	40	
FeMnNi	49	
Cr0.59Fe0.18CoNiMo0.18	32	Ming, K., Bi, X., & Wang, J. (2019). Strength and ductility of CrFeCoNiMo alloy with hierarchical microstructures. <i>International Journal of Plasticity</i>, 113, 255-268.
Al0.5CoCrCuFeNi	5	Tsai, C. W., Tsai, M. H., Yeh, J. W., & Yang, C. C. (2010). Effect of temperature on mechanical properties of Al0. 5CoCrCuFeNi wrought alloy. <i>Journal of Alloys and Compounds</i>, 490(1-2), 160-165.
CrFeNi2.1Al0.9	9.1	
CrFeNi2.2Al0.8	12.7	
CrFeNi2.3Al0.7	30	
CrFeNi2.4Al0.6	45	
CrFeNi2Al	6.4	
HfNbTaTiZr	15.7	Chen, S., Tseng, K. K., Tong, Y., Li, W., Tsai, C. W., Yeh, J. W., & Liaw, P. K. (2019). Grain growth and Hall-Petch relationship in a refractory HfNbTaZrTi high-entropy alloy. <i>Journal of Alloys and Compounds</i>, 795, 19-26.
Al0.3Cu0.5FeCrNi2	98	Zhang, K., Wen, H., Zhao, B., Dong, X., & Zhang, L. (2019). Precipitation behavior and its impact on mechanical properties in an aged carbon-containing Al0. 3Cu0. 5CrFeNi2 high-entropy alloy. <i>Materials Characterization</i>, 155, 109792.
CoCuFeMnNi	14	
CoCuFeMnNiSn0.03	18	Liu, L., Zhu, J. B., Li, L., Li, J. C., & Jiang, Q. (2013). Microstructure and tensile properties of FeMnNiCuCoSn_x high entropy alloys. <i>Materials & Design</i>, 44, 223-227.
HfNbTiZr	14.9	Wu, Y. D., Cai, Y. H., Wang, T., Si, J. J., Zhu, J., Wang, Y. D., & Hui, X. D. (2014). A refractory Hf25Nb25Ti25Zr25 high-entropy alloy with excellent structural stability and tensile properties. <i>Materials Letters</i>, 130, 277-280.
Al0.5Cr0.5FeNi	15.7	Dong, Y., Gao, X., Lu, Y., Wang, T., & Li, T. (2016). A multi-component AlCrFe2Ni2 alloy with excellent mechanical properties. <i>Materials Letters</i>, 169, 62-64.
Al0.3CoCrFeNi	48	Yasuda, H. Y., Miyamoto, H., Cho, K., & Nagase, T. (2017). Formation of ultrafine-grained microstructure in Al0. 3CoCrFeNi high entropy alloys with grain boundary precipitates. <i>Materials Letters</i>, 199, 120-123.
CoCuFeNi	15	Liu, L., Zhu, J. B., Zhang, C., Li, J. C., &

CoCuFeNiSn0.02	17	Jiang, Q. (2012). Microstructure and the properties of FeCoCuNiSn _x high entropy alloys. Materials Science and Engineering: A, 548, 64-68.
AlCoCrFeNi	1	Tang, Z., Senkov, O. N., Parish, C. M., Zhang, C., Zhang, F., Santodonato, L. J., ... & Liaw, P. K. (2015). Tensile ductility of an AlCoCrFeNi multi-phase high-entropy alloy through hot isostatic pressing (HIP) and homogenization. Materials Science and Engineering: A, 647, 229-240.
Al0.11Co0.51Cr0.51Cu0.11 Fe0.51Ni	30	Wang, Z. G., Zhou, W., Fu, L. M., Wang, J. F., Luo, R. C., Han, X. C., ... & Wang, X. D. (2017). Effect of coherent L1 ₂ nanoprecipitates on the tensile behavior of a fcc-based high-entropy alloy. Materials Science and Engineering: A, 696, 503-510.
V0.29Cr0.43Mn0.14Fe1Co 0.29Ni0.71	49	Asghari-Rad, P., Sathiyamoorthi, P., Bae, J. W., Moon, J., Park, J. M., Zargaran, A., & Kim, H. S. (2019). Effect of grain size on the tensile behavior of V10Cr15Mn5Fe35Co10Ni25 high entropy alloy. Materials Science and Engineering: A, 744, 610-617.
FeCoCrNiMn	54	Guo, L., Ou, X., Ni, S., Liu, Y., & Song, M. (2019). Effects of carbon on the microstructures and mechanical properties of FeCoCrNiMn high entropy alloys. Materials Science and Engineering: A, 746, 356-362.
Co0.99Cr0.95Fe0.93NiMn 0.91	46.2	Klimova, M. V., Shaysultanov, D. G., Zherebtsov, S. V., & Stepanov, N. D. (2019). Effect of second phase particles on mechanical properties and grain growth in a CoCrFeMnNi high entropy alloy. Materials Science and Engineering: A, 748, 228-235.
Al0.29Cr0.34FeMn0.65Ni0 .57	42.2	Elkatatny, S., Gepreel, M. A., Hamada, A., Nakamura, K., Yamanaka, K., & Chiba, A. (2019). Effect of Al content and cold rolling on the microstructure and mechanical properties of Al5Cr12Fe35Mn28Ni20 high-entropy alloy. Materials Science and Engineering: A, 759, 380-390.
Al0.14Cr0.34FeMn0.8Ni0. 57	48	
CoCrFeNiMo0.15	53.6	Wu, W., Guo, L., Guo, B., Liu, Y., & Song, M. (2019). Altered microstructural evolution and mechanical properties of CoCrFeNiMo0.15 high-entropy alloy by cryogenic rolling. Materials Science and Engineering: A, 759, 574-582.
FeMnCo0.25Cr0.25	55.7	Tang, K., Chen, L. B., Wang, S., Wei, R., Yang, Z. Y., Jiang, F., & Sun, J. (2019). Development of a large size FCC high-entropy alloy with excellent mechanical properties. Materials Science and

		Engineering: A, 761, 138039.
Co0.5CrFeNi1.5Ti0.3	46	Shun, T. T., & Chang, C. H. (2019). The effects of substitution of Co with Ni on microstructure, mechanical properties, and age hardening of Co _{1-x} CrFeNi _{1+x} Ti _{0.3} high-entropy alloys. <i>Materials Science and Engineering: A, 763, 138181.</i>
CoCrFeNiTi0.3	60	
CrFeNi2Ti0.3	37	
Al0.7CoCrFe2Ni	7.9	Wang, Q., Ma, Y., Jiang, B., Li, X., Shi, Y., Dong, C., & Liaw, P. K. (2016). A cuboidal B2 nanoprecipitation-enhanced body-centered-cubic alloy Al _{0.7} CoCrFe ₂ Ni with prominent tensile properties. <i>Scripta Materialia, 120, 85-89.</i>
Co1.75Cr0.75FeNiMo0.5	21.9	Ming, K., Bi, X., & Wang, J. (2017). Precipitation strengthening of ductile Cr ₁₅ Fe ₂₀ Co ₃₅ Ni ₂₀ Mo ₁₀ alloys. <i>Scripta Materialia, 137, 88-93.</i>
Al0.3CoCrFeNi	65	Gwalani, B., Gorsse, S., Choudhuri, D., Zheng, Y., Mishra, R. S., & Banerjee, R. (2019). Tensile yield strength of a single bulk Al _{0.3} CoCrFeNi high entropy alloy can be tuned from 160 MPa to 1800 MPa. <i>Scripta Materialia, 162, 18-23.</i>
CoFeNi2V0.5Mo0.2	119.5	Jiang, L., Lu, Y. P., Song, M., Lu, C., Sun, K., Cao, Z. Q., ... & Wang, L. M. (2019). A promising CoFeNi ₂ V _{0.5} Mo _{0.2} high entropy alloy with exceptional ductility. <i>Scripta Materialia, 165, 128-133.</i>
AlCoCrFeNi2.1	21.4	Shi, P., Ren, W., Zheng, T., Ren, Z., Hou, X., Peng, J., ... & Liaw, P. K. (2019). Enhanced strength-ductility synergy in ultrafine-grained eutectic high-entropy alloys by inheriting microstructural lamellae. <i>Nature communications, 10(1), 1-8.</i>
Hf0.5Nb0.5Ta0.5Ti1.5Zr	19	Sheikh, S., Shafeie, S., Hu, Q., Ahlström, J., Persson, C., Veselý, J., ... & Guo, S. (2016). Alloy design for intrinsically ductile refractory high-entropy alloys. <i>Journal of applied physics, 120(16), 164902.</i>
Co0.2Cr0.2FeMn0.6	75	Li, Z., Tasan, C. C., Pradeep, K. G., & Raabe, D. (2017). A TRIP-assisted dual-phase high-entropy alloy: grain size and phase fraction effects on deformation behavior. <i>Acta Materialia, 131, 323-335.</i>
Co1.75Cr1.25FeNi	96.2	Wei, D., Li, X., Heng, W., Koizumi, Y., He, F., Choi, W. M., ... & Chiba, A. (2019). Novel Co-rich high entropy alloys with superior tensile properties. <i>Materials Research Letters, 7(2), 82-88.</i>
Co3Cr1.67FeNi	76.1	
NbTaTi	18.5	Zýka, J., Málek, J., Veselý, J., Lukáč, F., Čížek, J., Kuríplach, J., & Melikhova, O. (2019). Microstructure and room temperature mechanical properties of
NbTaTiZr	6.4	

		different 3 and 4 element medium entropy alloys from HfNbTaTiZr system. Entropy, 21(2), 114.
Al0.28Co0.69Cr0.22Fe0.42 NiTi0.17	27	Haas, S., Manzoni, A. M., Krieg, F., & Glatzel, U. (2019). Microstructure and mechanical properties of precipitate strengthened high entropy alloy Al10Co25Cr8Fe15Ni36Ti6 with additions of hafnium and molybdenum. Entropy, 21(2), 169.
CoCrFeNiMo0.2	53	Zhang, C., Liu, B., Liu, Y., Fang, Q., Guo, W., & Yang, H. (2019). Effects of Annealing on Microstructure and Mechanical Properties of Metastable Powder Metallurgy CoCrFeNiMo0.2 High Entropy Alloy. Entropy, 21(5), 448.

References

- [1] W. Huang, P. Martin, and H. L. Zhuang, *Acta Mater.*, 2019, **169**, 225-236.
- [2] N. Islam, W. Huang, and H. L. Zhuang, *Comput. Mater. Sci.*, 2018, **150**, 230-235.
- [3] Li, J, B. Xie, Q. Fang, B. Liu, Y. Liu, and P. K. Liaw, *J. Mater. Sci. Technol.*, 2021, **68**, 70-75.
- [4] C. Varvenne, G. P. M. Leyson, M. Ghazisaeidi, and W. A. Curtin, *Acta Mater.*, 2017, **124**, 660-683.
- [5] F. Maresca, and W. A. Curtin, *Acta Mater.*, 2020, **182**, 144-162.
- [6] T. Sathish, S. Rangarajan, A. Muthuram, and R. P. Kumar, *Mater. Today: Proc.*, 2020, **21**, 108-112.
- [7] X. Geng, H. Wang, W. Xue, S. Xiang, H. Huang, L. Meng, and G. Ma, *Comput. Mater. Sci.*, 2020, **171**, 109235.
- [8] J. M. Barrios, and P. E. Romero, *Materials*, 2019, **12**, 2574.
- [9] R. F. Martinez, A. Okariz, J. Ibarretxe, M. Iturrondobeitia and T. Guraya, *Comput. Mater. Sci.*, 2014, **92**, 102-113.
- [10] J. Y. He, W. H. Liu, H. Wang, Y. Wu, X. J. Liu, T.G.Nieh and Z.P. Lu, *Acta Mater.*, 2014, **62**, 105-113.
- [11] Z. Pei, J. Yin, J. A. Hawk, D. E. Alman and M.C. Gao, *npj Comput. Mater.*, 2020, **6**, 1-8.
- [12] C. Wang, H.Fu, L. Jiang, D. Xue and J. Xie, *npj Comput. Mater.*, 2019, **5**, 1-8.
- [13] Y. Zhang, Y. J. Zhou, J. P. Lin, G. L. Chen and P. K. Liaw, *Adv. Eng. Mater.*, 2008, **10**, 534-538.
- [14] X. Yang, and Y. Zhang, *Mater. Chem. Phys.*, 2012, **132**, 233-238.
- [15] S. Guo, C.Ng, J. Lu, and C.T. Liu, *J. Appl. Phys.*, 2011, **109**, 103505.
- [16] Z.Wang, Y. Huang, Y. Yang, J. Wang and C.T. Liu, *Scr. Mater.*, 2015, **94**, 28-31.
- [17] A. K. Singh, N. Kumar, A. Dwivedi and A.Subramaniam, *Intermetallics*, 2014, **53**, 112-119.
- [18] L. A. Gypen and A. Deruyttere, *J. Mater. Sci.*, 1977, **12**, 1028-1033.
- [19] O. N.Senkov, J. M. Scott, S. V. Senkova, D. B. Miracle, C. F. Woodward, *J. Alloys Compd.*, 2011, **509**, 6043-6048.

- [20] I. Toda-Caraballo and P. E. J. Rivera-Díaz-del-Castillo, *Acta Mater.*, 2015, **85**, 14-23.
- [21] O. N. Senkov, J. M. Scott, S. V. Senkova, F. Meisenkothen, D. B. Miracle and C. F. Woodward, *J. Mater. Sci.*, 2012, **47**, 4062-4074.
- [22] Q. Wang, Y. Ma, B. Jiang, X. Li, Y. Shi, C. Dong and P. K. Liaw, *Scr. Mater.*, 2016, **120**, 85-89.
- [23] Y. Lu, X. Gao, L. Jiang, Z. Chen, T. Wang, J. Jie, H. Kang, Y. Zhang, S. Guo and H. Ruan, *Acta Mater.*, 2017, **124**, 143-150.
- [24] D. Wei, X. Li, W. Heng, Y. Koizumi, F. He, W. M. Choi, B. J. Lee, H. S. Kim, H. Kato and A. Chiba, *Mater. Res. Lett.*, 2019, **7**, 82-88.
- [25] X. Jin, J. Bi, L. Zhang, Y. Zhou, X. Du, Y. Liang and B. Li, *J. Alloys Compd.*, 2019, **770**, 655-661.
- [26] S. Elkhatatny, M. A. H. Gepreel, A. Hamada, K. Nakamura, K. Yamanaka and A. Chiba, *Mater. Sci. Eng. A*, 2019, **759**, 380-390.
- [27] A. Shabani, M. R. Toroghinejad, A. Shafyei and R.E. Logé, *Mater. Chem. Phys.*, 2019, **221**, 68-77.
- [28] U. Sunkari, S. R. Reddy, S. Chatterjee and P. P. Bhattacharjee, *Mater. Lett.*, 2019, **248**, 119-122.
- [29] L. Liu, J. B. Zhu, L. Li, J. C. Li and Q. Jiang, *Mater. Des.*, 2013, **44**, 223-227.
- [30] L. Liu, J.B. Zhu, C. Zhang, J. C. Li and Q. Jiang, *Mater. Sci. Eng. A*, 2012, **548**, 64-68.
- [31] J. Zýka, J. Málek, J. Veselý, F. Lukáč, J. Čížek, J. Kuriplach and O. Melikhova, *Entropy*, 2019, **21**, 114.
- [32] C. Wen, Y. Zhang, C. Wang, D. Xue, Y. Bai, S. Antonov, L. Dai, T. Lookman and Y. Su, *Acta Mater.*, 2019, **170**, 109-117.
- [33] R. Feng, M. C. Gao, C. Zhang, W. Guo, J. D. Poplawsky, F. Zhang, J. A. Hawk, J. C. Neufeind, Y. Ren and P. K. Liaw, *Acta Mater.*, 2018, **146**, 280-293.
- [34] B. D. Conduit, N. G. Jones, H. J. Stone and G. J. Conduit, *Mater. Des.*, 2017, **131**, 358-365.
- [35] C. H. Caceres, *Metall. Mater. Trans. A*, 2007, **38**, 1649-1662.
- [36] P. Peng, X. He, J. She, A. Tang, M. Rashad, S. Zhou, G. Zhang, X. Mi and F. Pan, *Mater. Sci. Eng. A*, 2019, **766**, 138332.
- [37] A. T. Abbas, M. Abubakr, M. A. Hassan, M. Luqman, M. S. Soliman and H. Hegab, *J. Mater. Res. Technol.*, 2020, **9**, 14568-14581.

[38] D. Qiao, Y. Lu, Z. Tang, X. Fan, T. Wang T. Li, and P K. Liaw, *Int. J. Hydrogen Energy*, 2019, **44**, 3527-3537.